平成30年度　修士論文

Compressed-Sensing-Aided Subcarrier In-phase/Quadrature-phase Index Modulation and Its Efficient Detector

圧縮サブキャリアIQインデックス変調とその効率的復調法に関する研究

学籍番号　1731031

氏　名　大比良　和哉

指導教員　石橋　功至 准教授

電気通信大学　情報理工学研究科

情報・ネットワーク工学専攻

提出日　平成31年1月28日

修士論文の和文要旨

研究科・専攻	大学院　情報理工学研究科　情報・ネットワーク工学専攻　博士前期課程		
氏　　名	大比良　和哉	学籍番号	1731031
論文題目	圧縮サブキャリア IQ インデックス変調と その効率的復調法に関する研究		

要旨

圧縮センシングを用いたサブキャリアインデックス変調 (CS-SIM: Compressed-Sensing-aided Subcarrier Index Modulation) では，サブキャリアインデックス変調 (SIM: Subcarrier Index Modulation) 信号の疎性を用いた効率的な復調を行なっておらず，圧縮信号から SIM 信号を再構成するために多くの演算量を要する．信号の疎性のみならず離散性を考慮した低演算量の再構成アルゴリズムとして，離散性を考慮した高速反復縮退アルゴリズム (DFISTA: Discreteness-aware Fast Iterative Shrinkage-Thresholding Algorithm) が提案されているが，DFISTA は実数信号に対してのみ有効であるため，実軸・虚軸成分に強い相関を持つ SIM 信号の再構成には適さない．そこで本研究では，実軸・虚軸成分をそれぞれ独立に SIM を施すサブキャリア IQ インデックス変調 (SIQIM: Subcarrier In-phase/Quadrature-phase Index Modulation) に対して CS を適用した圧縮サブキャリア IQ インデックス変調 (CS-SIQIM) を提案する．SIQIM 信号は実軸・虚軸成分が独立であるため，劣化なしで等価実数表現することが可能であり，DFISTA による効率的な再構成を行うことが可能である．さらに，DFISTA の再構成特性を向上させるために，複数の SIQIM 信号を一括して圧縮を行う一括圧縮サブキャリア IQ インデックス変調 (AC-SIQIM: Aggregate-Compression aided SIQIM) を提案する．また，DFISTA のハイパーパラメータの最適化のために，差分進化法に基づく最適化手法を提案する．本論文では，従来の CS-SIM と比較して，CS-SIQIM が低演算量でありながらほぼ同等のビット誤り率 (BER: Bit-Error Rate) を持ち，一括圧縮 (AC: Aggregate-Compression) によって，CS-SIQIM の BER 特性が改善可能であることを計算機シミュレーションより示す．

Abstract

Compressed-Sensing-aided subcarrier in-phase/quadrature index modulation (CS-SIQIM) and aggregate-compression aided SIQIM (AC-SIQIM) relying on discreteness-aware fast iterative shrinkage-thresholding algorithm (DFISTA) are proposed. To significantly increase its bandwidth efficiency, we invoke compressed sensing (CS) for conveying independent information bits via the in-phase and quadrature-phase signals of subcarrier index modulation (SIM). The conventional CS-SIM detector imposes an exponential complexity with the size of SIM symbol. To lower the complexity for the detection, the abovementioned DFISTA, which exploits both the sparsity and the discrete nature of the SIQIM signals, is employed. Furthermore, in AC-SIQIM, SIQIM signals are jointly compressed by a linear matrix, which is so-called aggregate compression to improve the reconstruction performance of DFISTA. Moreover, in order to apply high-order modulation to CS-SIQIM and AC-SIQIM, hyperparameters of DFISTA are optimized via differential evolution. We evaluate the proposed CS-SIQIM in terms of both its bit-error rate (BER) and computational complexity performance and show that aggregate compression (AC) improves the BER performance of CS-SIQIM. Finally, we show that AC-SIQIM employing high-order modulation is capable of outperforming conventional OFDM.

Contents

List of Figures

List of Tables

Chapter 1

Introduction

1.1 Background

In the operational wireless communication systems, orthogonal frequency division multiplexing (OFDM) is employed as a benefit of its high bandwidth efficiency and robustness against frequency selective fading. Recently, OFDM combined with index modulation (IM), namely, subcarrier index modulation (SIM) has been proposed in [1], where specific patterns of activated subcarriers implicitly convey information in addition to classical modulated symbols. SIM is a frequency-domain variant of the general concept of IM. This general IM family also includes the popular spatial modulation (SM) [2] and generalized spatial-frequency index modulation [3]. Since SIM inherits the characteristics of OFDM and has the flexibility of transmission rate, it is an attractive and promising wireless transmission scheme. The main limitation of SIM is however that it can only outperform OFDM at low bandwidth efficiency because the minimum Euclidean distance (MED) of SIM symbols is reduced upon increasing the number of IM symbols relying on the activated subcarriers [4]. To improve the bandwidth efficiency, Xiao et al. proposed SIM with subcarrier interleaver [5], which outperforms the conventional SIM over correlated channels since the frequency-domain interleaver decorrelates the channels. Also, dual-mode IM aided OFDM has been proposed in [6]. This scheme employs two different modulation schemes such as quadrature phase shift keying (QPSK) and $\pi/4$-shift QPSK to improve the bandwidth efficiency and exhibit the superior performance to the conventional SIM. However, the improvements via both schemes [5, 6] are not significant compared with the conventional SIM.

Recently, compressed-sensing (CS)-aided SIM (CS-SIM) has been presented, which significantly improves both the bandwidth and energy efficiency, and a so-called iterative residual check (IRC) detector has been proposed in [7]. While the performance of CS-SIM with the IRC detector is superior to that of both conventional SIM and OFDM, the detector relies on matrix inversions in each iteration and requires potentially excessive complexity as increasing the number of active subcarriers to raise its transmission rate. Moreover, it is worth noting that IRC detector does not exploit the inherent sparsity of

SIM signals to reduce the complexity of the detection where the concept is to accurately estimate a high-dimensional sparse vector from a small number of measurements [8]. SIM signals have inherent sparsity because only a few subcarriers are activated for data transmission. Therefore, it is a natural consequence to combine CS-based detector with SIM for decreasing the computational complexity.

As an efficient CS algorithm, discreteness-aware approximate message passing (DAMP) algorithm has been proposed [9, 10]. This algorithm invokes the sum-of-absolute-values (SOAV) optimization [11] besides $l_1 - l_2$ optimization so as to efficiently estimate discrete-valued signals with sparsity. It has been shown that the algorithm outperforms the conventional approximate message passing (AMP) [12] in terms of mean square error (MSE) when original signals exhibit discreteness. While the algorithm seems to be appropriate for detecting SIM signals, it is available only for real-valued signals. Note that SIM signals should not be transformed into a real-valued representation since when either in- or quadrature-component takes a non-zero value, the other component must take the value too. This correlation cannot be taken into account in the original DAMP algorithm. Moreover, in CS-SIM, a measurement matrix is distorted by channel coefficient, so that the assumption that variances of all elements in a measurement matrix are constant is not satisfied. As a result, DAMP algorithm is not applicable for CS-SIM system with a straightforward manner.

In contrast to DAMP algorithm, fast iterative shrinkage-thresholding algorithm (FISTA) [13] has a good reconstruction performance even over fading channels since this algorithm has no constraint of a construction of a measurement matrix. As similar to DAMP algorithm, discreteness-aware FISTA (DFISTA) has been proposed for faster-than-Nyquist scenario in [14], which simultaneously solves $l_1 - l_2$ and SOAV optimization. While DFISTA is applicable even to CS-SIM scenario, DFISTA can also treat real-valued signals. It therefore cannot be directly applied to CS-SIM scenario.

Against the aforementioned background, we propose CS aided subcarrier in-phase/quadrature-phase index modulation (CS-SIQIM) relying on DFISTA so as to improve the bandwidth efficiency and efficiently detect subcarrier in-phase/quadrature-phase index modulation (SIQIM) signals. SIQIM can be regarded as generalized OFDM with index modulation since in-phase and quadrature-phase signals in SIQIM are independently modulated by the classical SIM. Therefore, complex SIQIM signals can be represented by real-valued signals with no degradation. This IQ-independent structure allows the receiver to independently detect the signals in each domain. Moreover, according to Welch bound which determines the reconstruction performance of CS algorithm [15], the performance depends on the compression size. Hence, we propose aggregate-compression-aided SIQIM (AC-SIQIM) in which SIQIM signals are jointly compressed by a linear matrix to improves the performance, which is referred to as *aggregate compression* (AC) throughout the paper. Furthermore, thanks to the IQ-independent structure, the size of the linear compression can be doubled through real-valued representation. We further propose an optimization method based on differential evolution (DE)[16] to optimize hyperparameters in DFISTA in order to apply high-order modulation to AC-SIQIM. Com-

puter simulations show that our proposed CS-SIQIM has comparable bit-error rate (BER) performance to CS-SIM with low complexity. Moreover, our proposed AC-SIQIM outperforms both conventional OFDM, SIM, and CS-SIM and outperforms OFDM with high-order modulations.

1.2 Organization

The rest of this paper is organized as follows. The detail and problem of SIM are shown in Chapter 2. In Chapter 3, the conventional CS-based SIM is introduced. Then, our proposed CS-based SIQIM system is described in detail in Chapter 4. In Chapter 5 the computational complexity is evaluated by comparing the conventional detectors, and the BER performance is evaluated via computer simulation. Chapter 6 concludes the paper.

1.3 Notations

Throughout this paper, we use the following notations. A column vector and a matrix are represented by $\mathbf{w}$ and $\mathbf{W}$, respectively. A vector whose elements are all 1 is represented by $\mathbf{1}$. For N-dimensional column vector $\mathbf{w}$, the l_1 and l_2 norms are defined as $||\mathbf{w}||_1 = \sum_{i=1}^{N} |w_i|$ and $||\mathbf{w}||_2 = \sum_{i=1}^{N} \sqrt{w_i^2}$, respectively. $(\cdot)^{\mathrm{T}}$ and $(\cdot)^{\mathrm{H}}$ stand for the transpose and the conjugate transpose, respectively. The imaginary unit is represented by j. $\mathfrak{R}(\mathbf{w}) \in \mathbb{R}^N$ and $\mathfrak{I}(\mathbf{w}) \in \mathbb{R}^N$ denote real and imaginary parts of a complex column vector $\mathbf{w}$, respectively. Furthermore, $\mathcal{CN}(0,1)$ denotes a complex Gaussian distribution with zero mean and unit variance. The binomial coefficient of N and K is represented by $\binom{N}{K}$, where $N \geq K$. Floor function is represented by $\lfloor \cdot \rfloor$. $\mathbb{E}[\cdot]$ denotes the expectation operation.

Chapter 2

Subcarrier Index Modulation

The combination of OFDM and index modulation, named SIM, is inherently attractive for wireless communications since the modulation is capable of outperforming the conventional OFDM in terms of BER performance. SIM is a family of generalized index modulation in frequency-domain, so that active subcarrier patterns are regarded as an index and convey information bits as well as data symbol. Figure 2.1,2.2 show power spectrum density of OFDM and SIM. As shown in Fig. 2.2, since not all subcarriers are employed for data symbol transmission in SIM, SIM obtains power gain against OFDM and has larger MED than OFDM.

2.1 Transmitter

In contrast to OFDM, SIM performs on multiple subcarriers. Let N and K denote the number of subcarriers and the number of active subcarriers in a SIM signal, respectively,

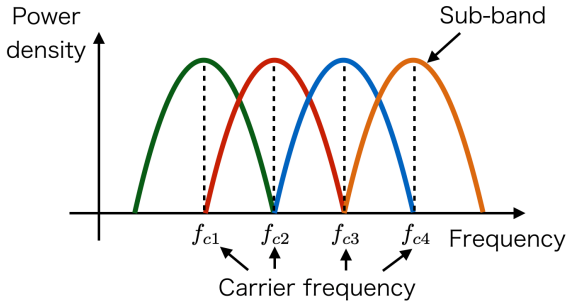

Figure 2.1: Power spectrum of OFDM signal

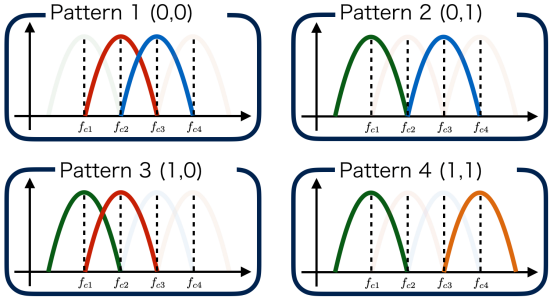

Figure 2.2: Power spectrum of SIM signal where 2 out of 4 subcarriers are activated.

so that K out of N subcarriers are activated. Therefore, SIM signal is expressed as

$$\mathbf{x} = [0, ..., \underbrace{x_1}_{u_1-\text{th}}, ..., \underbrace{x_K}_{u_K-\text{th}}, ..., 0]^{\mathrm{T}} \in \mathbb{C}^N, \tag{2.1}$$

where $x_i \in \mathcal{X}$ $(i = 1, ..., K)$ and $\mathbf{u} \in \mathcal{I} \subset \{1, ..., N\}^K$ are classical data symbol and subcarrier index, respectively, where $\mathcal{X} \subset \mathbb{C}$ is a set of L-ary constellation symbols and $\mathcal{I}$ is a set of possible subcarrier index patterns. In SIM, information bits can be conveyed via index pattern as well as classical However, only $\lfloor \log_2(\Delta) \rfloor$ index patterns are employed for corresponding to information bits. Therefore, the number of information bits per subblock and its transmission rate are given by

$$B = \lfloor \log_2(\Delta) \rfloor + K \log_2 L \tag{2.2}$$

and

$$R = B/N \tag{2.3}$$

, respectively.

The SIM signal is converted into a time-domain signal via inverse fast Fourier tranform (IFFT), then cyclic prefix (CP) is addded into the time-domain signal. Finally, a CP-added time-domain signal is transmitted.

2.2 Receiver

Here we consider independent and identically distributed (i.i.d.) frequency-flat Rayleigh fading channels for the sake of simplicity. Therefore, after removal of CP and fast Fourier transform (FFT), a frequency-domain received signal can be represented by

$$\mathbf{y} = \mathbf{H}\mathbf{x} + \mathbf{n} \in \mathbb{C}^N, \tag{2.4}$$

where $\mathbf{H} \in \mathbb{C}^{N \times N}$ is a diagonal channel matrix whose diagonal elements follow $\mathcal{CN}(0, 1)$ and $\mathbf{n} \in \mathbb{C}^N$ is additive white Gaussian noise (AWGN) vector whose elements follow $\mathcal{CN}(0, N_0)$ where N_0 is the single-side noise spectral density.

SIM signals convey information bits via subcarrier index patterns and data symbols, so that these patterns and symbols should be jointly estimated for the received signal $\mathbf{y}$. According to [4], the optimal detector is joint maximum likelihood (JML) detector, which is given by

$$\hat{\mathbf{x}} = \underset{\mathbf{x} \in \mathcal{X}^K \times \mathcal{I}}{\arg\min} ||\mathbf{y} - \mathbf{H}\mathbf{x}||_2^2. \tag{2.5}$$

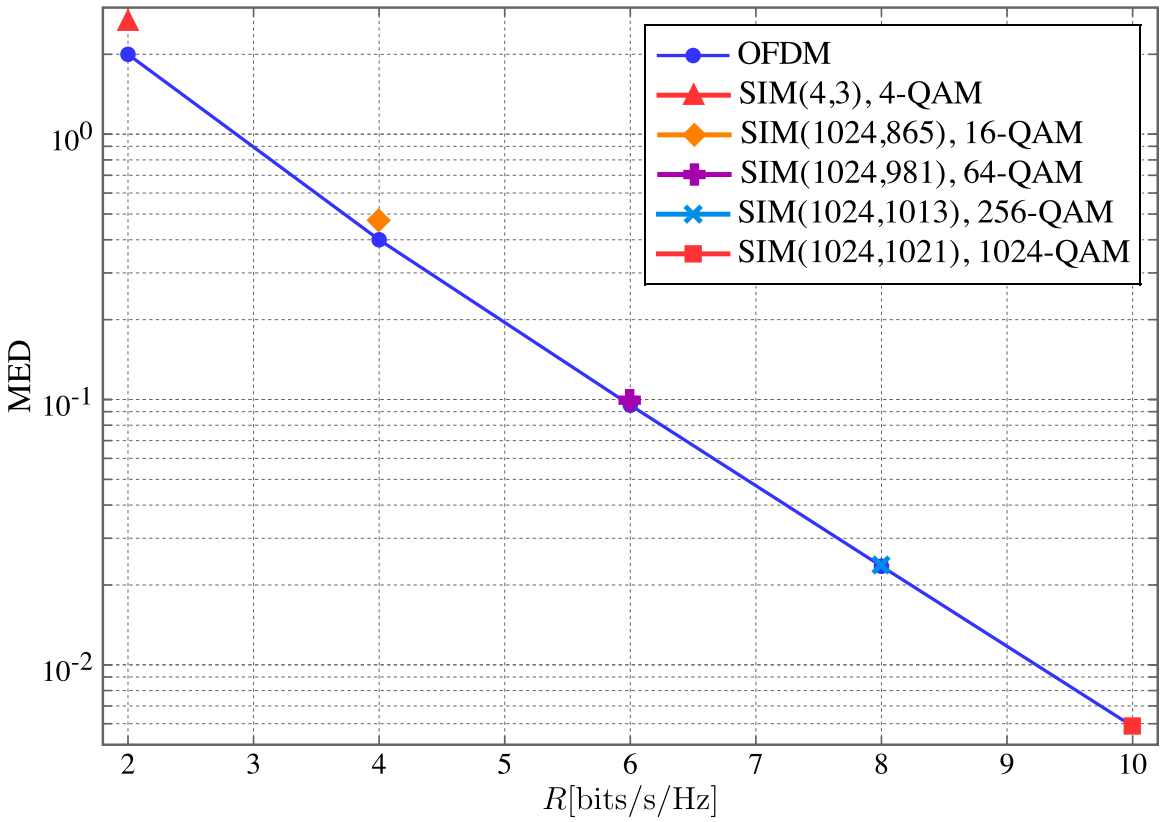

Figure 2.3: MED v.s. transmission rate of SIM and OFDM where square QAM is employed in both schemes and the notation "SIM(N,K)" denotes SIM in which K out of N subcarriers are activated.

2.3 MED comparison between SIM and OFDM

In this section, we evaluate the MED of SIM signals since BER performance significantly depends on its MED of modulated signals in uncoded scenarios. Naoki et al. [4] have derived the MED of SIM signals, which can be regarded as a function whose arguments are the number of subcarriers N and the number of active subcarriers K, and the number of signal points in a constellation L. Therefore, the MED function for square quadrature-amplitude-modulation (QAM) is represented by

$$\mathrm{MED}(N, K, L) = \frac{6N}{K(L-1)}. \tag{2.6}$$

The MED of OFDM signals emploing square QAM coincides (2.6) with $N = K$.

Figure 2.3 shows the MEDs of SIM and OFDM signals employing square QAM. The parameters of SIM signals (N, K, L) are designed based on Criterion 1,2 in [4]. As shown in Fig. 2.3, the MED of SIM signals is greater than that of OFDM with a low transmission

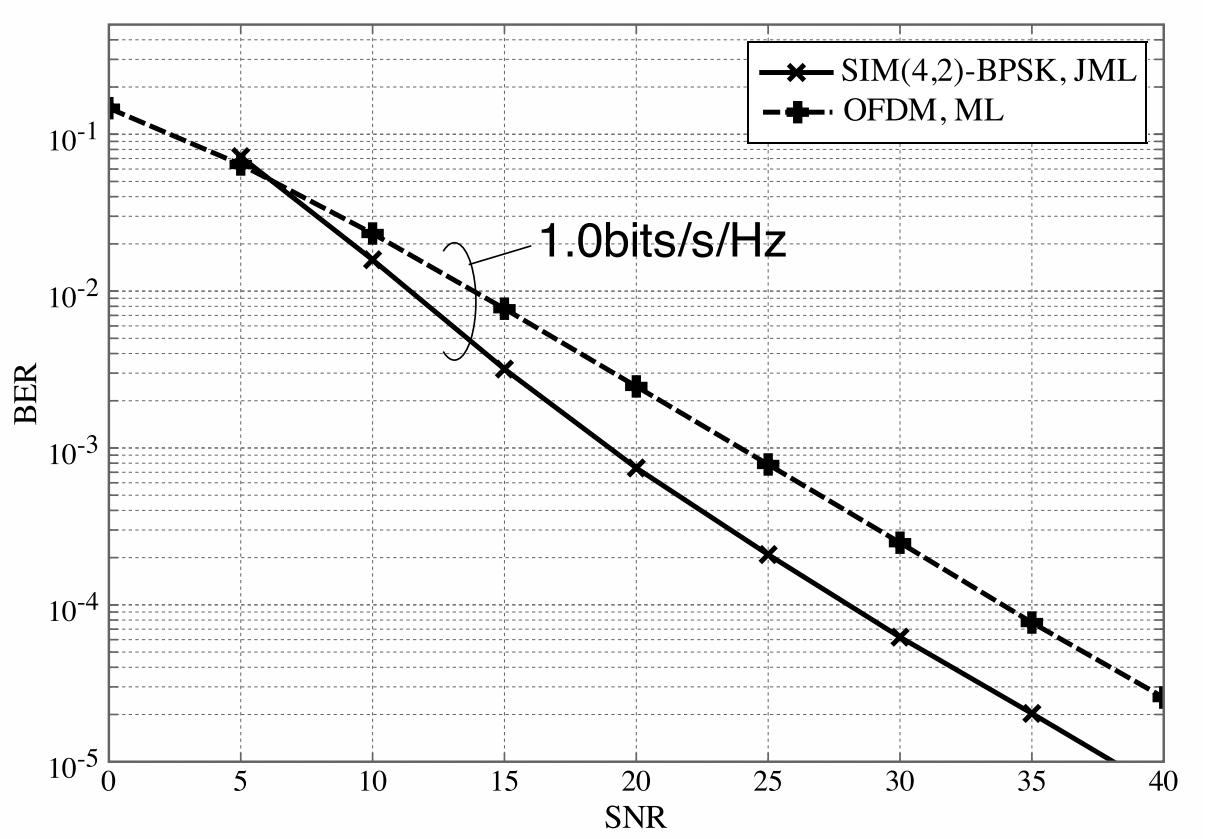

Figure 2.4: BER performances of SIM and OFDM where

rate. However, with a high transmission rate, the difference between the MEDs decreases since the power gain of SIM signals against OFDM signals decreases by employing most of the subcarriers for data symbol transmission.

2.4 BER evaluation

Figures 2.4 and 2.5 show the BER performances of OFDM and SIM over frequency-selective Rayleigh fading channels where the transmission rates are set as 1.0 and 2.0 bits/s/Hz, respectively. Moreover, binary phase shift keying (BPSK) and QPSK is employed in Figs. 2.4 and 2.5. In addition, maximum likelihood (ML) and JML detection are employed for OFDM and SIM, respectively. As the aforementioned fact that MED of SIM is larger than that of OFDM with the aid of the power gain, the BER performance of SIM is better than that of OFDM at high signal-to-noise power ratio (SNR) region in both figures. However, comparing the BER performances in two figures, the superiority of SIM over OFDM in terms of BER performance is degraded when the transmission rate increases.

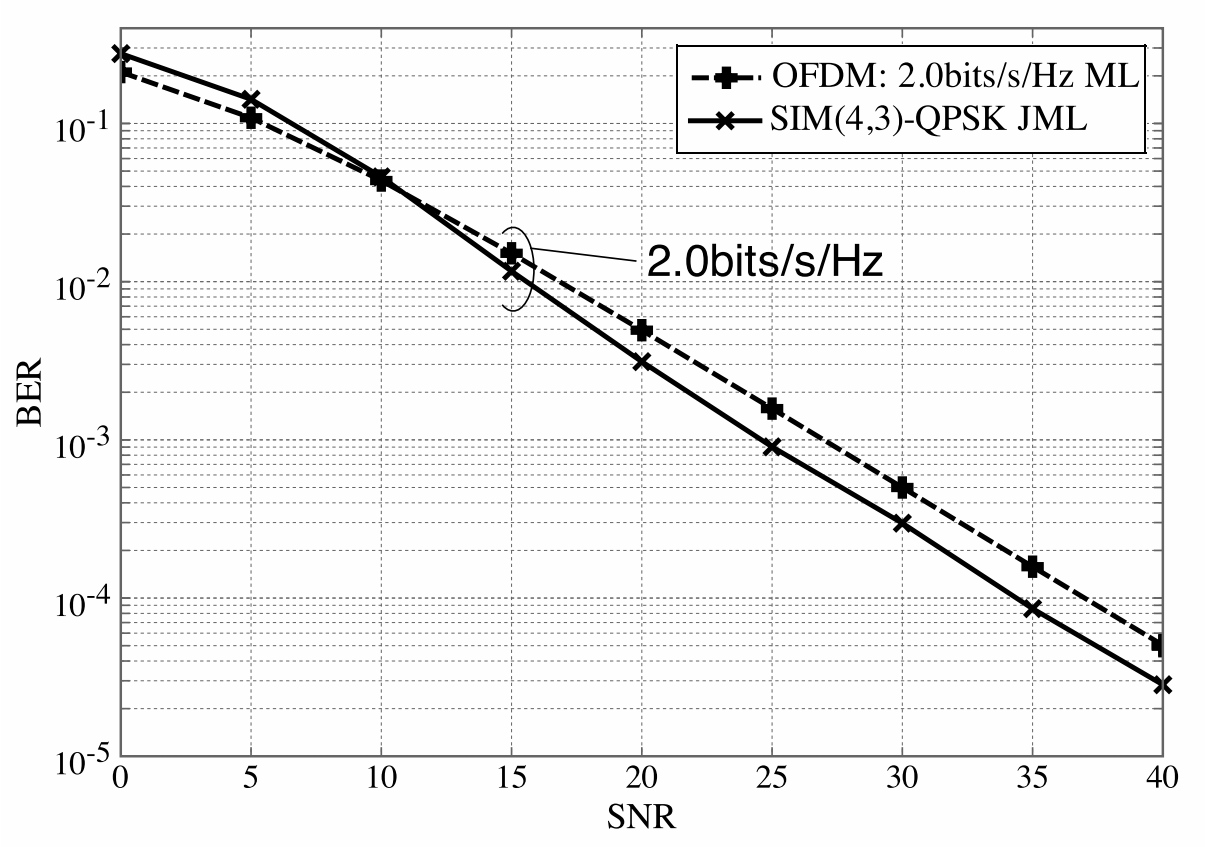

Figure 2.5: BER comparison of OFDM and SIM over frequency-selective Rayleigh fading channels where the transmission rates are set as 2.0 bits/s/Hz.

2.5 Chapter conclusions

In this chapter, we briefly introduced SIM and show the MED and BER performance. As shown in this chapter, SIM has superiority over OFDM in terms of BER performance with low transmission rate since the power gain against OFDM signals can be obtained by employing a part of OFDM subcarriers for data symbol transmission. However, at a high transmission rate, the superiority is degraded, which can be predicted by Fig. 2.3. Therefore, a technique to increase the transmission rate of SIM while keeping the superiority over OFDM is required. In the next chapter, CS-SIM, which can increase the transmission rate and outperforms SIM and OFDM in terms of BER performance, will be explained.

Chapter 3

Conventional CS-based SIM system

In this chapter, we introduce the conventional CS-SIM system and show that CS-SIM outperforms conventional OFDM in terms of BER performance.

3.1 System model

Figure 3.1 shows the system model of conventional CS-SIM. We assume M_{all} subcarriers in every OFDM symbol and these subcarriers are divided into G subblocks, so that each subblock has $M = M_{\text{all}}/G$ subcarriers. Note that we assume N *virtual*-domain subcarriers per subblock, and SIM signals are generated in the virtual domain and K out of N virtual subcarriers are activated where $N > M$ and $N \gg K$. Although the number of possible index patterns is $\Delta = \binom{N}{K}$, only $\lfloor \log_2 \Delta \rfloor$ index patterns are employed. In every subblock, the information-bit vector $\mathbf{p}_g \in \{0,1\}^B$ is used for generating the SIM signal $\mathbf{x}_g \in \mathbb{C}^N$ at the g-th subblock where B is the number of transmitted information bits per subblock, then the SIM signal is compressed into an M-dimensional frequency-domain signal $\mathbf{s}_g \in \mathbb{C}^M$ as follows:

$$\mathbf{s}_g = \mathbf{A}\mathbf{x}_g \tag{3.1}$$

where $\mathbf{A} \in \mathbb{C}^{M \times N}$ is a measurement matrix. Therefore, the transmission rate of CS-SIM is given by

$$R = (\lfloor \log_2 \Delta \rfloor + K \log_2 L)/M. \tag{3.2}$$

Note that, compared with (2.3), the transmission rate of CS-SIM is greater than that of SIM with fixed parameters. All the frequency-domain signals are gathered into a serial signal, then the serial signal is transformed into a time-domain signal via IFFT and added CP. Finally, CP-added time-domain signal $\mathbf{s}_{\text{T}}$ is transmitted.

At the receiver side, CP is removed from the received time-domain signal $\mathbf{y}_{\text{T}}$ and the time-domain signal is transformed into a frequency-domain signal via FFT. We assume that wireless channels are frequency-selective Rayleigh fading channels, so that the

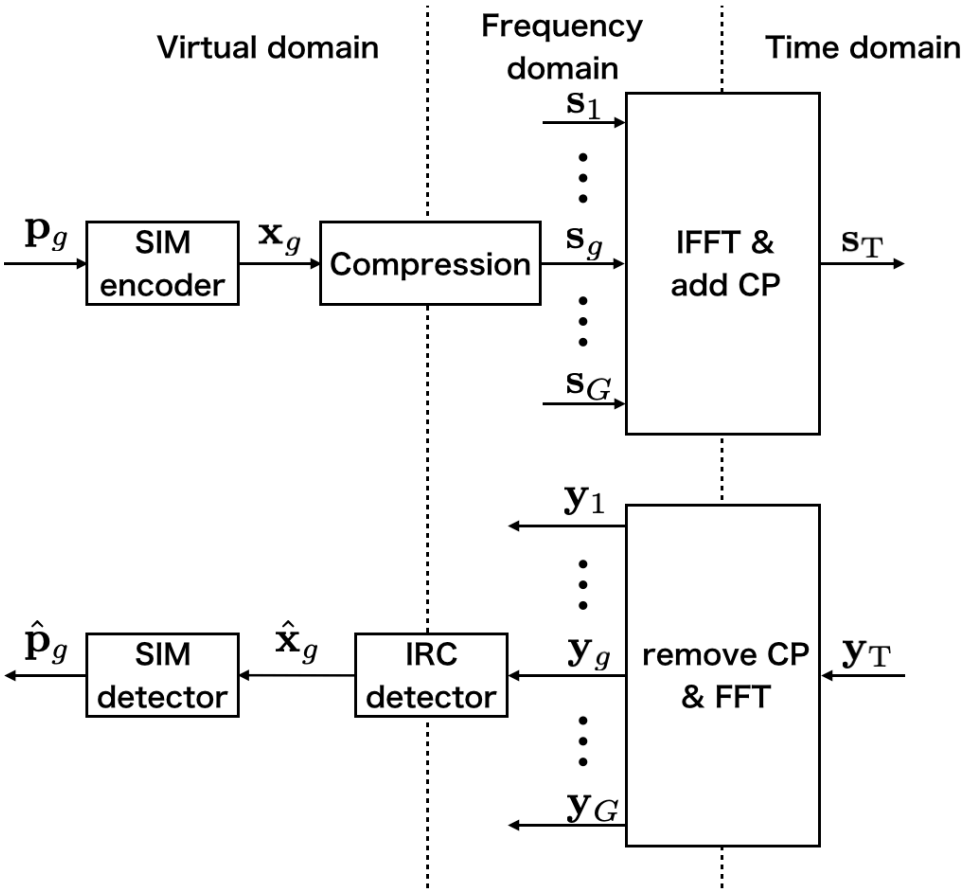

Figure 3.1: System model of conventional CS-SIM employing IRC detector

frequency-domain received signal at the g-th subblock is expressed as

$$\mathbf{y}_g = \mathbf{H}_g \mathbf{s}_g + \mathbf{n}_g \tag{3.3}$$
$$= \mathbf{H}_g \mathbf{A} \mathbf{x}_g + \mathbf{n}_g \tag{3.4}$$
$$= \mathbf{\Phi}_g \mathbf{x}_g + \mathbf{n}_g, \tag{3.5}$$

where $\mathbf{H}_g$ is a diagonal channel matrix whose diagonal elements follow $\mathcal{CN}(0,1)$ and $\mathbf{n}_g$ is AWGN vector whose elements follow $\mathcal{CN}(0,N_0)$ where N_0 is the single-side noise spectral density. IRC detector estimates the SIM signal $\mathbf{x}_g$ from the frequency-domain received signal $\mathbf{y}_g$, which is can be regarded as an estimation of high-dimensional vector from its low-dimensional measurement vector, i.e., underdetermined problem. The detail of IRC detector is explained in the next section. Finally, SIM detector converts an estimated SIM signal $\hat{\mathbf{x}}_g \in \mathbb{C}^N$ into the corresponding bits vector $\hat{\mathbf{p}}_g \in \{0,1\}^B$.

3.2 IRC detector

For the sake of simplicity of notation, we omit the subscript "g" in this section. IRC detector is characterized by two estimation part: minimum mean-square-error (MMSE) estimation and JML detection. The first estimation is based on MMSE estimation, which is expressed as

$$\hat{\mathbf{x}} = (\mathbf{\Phi}^{\mathrm{H}}\mathbf{\Phi} + N_0 \mathbf{I}_M)^{-1} \mathbf{\Phi}^{\mathrm{H}} \mathbf{y} \in \mathbb{C}^N, \tag{3.6}$$

where $\mathbf{I}_M$ is a $M \times M$ identity matrix. Then, the resulted MMSE estimates are ordered by thier power as

$$|\hat{x}(i_1)|^2 \geq |\hat{x}(i_2)|^2 \geq \cdots \geq |\hat{x}(i_N)|^2. \tag{3.7}$$

The index with the largest power is chosen, and the first index subset $\mathcal{I}_1 = \{\breve{\mathbf{u}}_{1,1}, ..., \breve{\mathbf{u}}_{1,C_1}\} \subset \mathcal{I}$ is generated where all the index patterns $\breve{\mathbf{u}}_{1,c_1}$ contain the first chosen index i_1. For each index pattern in the subset, Moore-Penrose pseudo-inverse matrix is calculated, which is represented by

$$\mathbf{\Phi}^{\dagger}_{\breve{\mathbf{u}}_{1,c_1}} = (\mathbf{\Phi}^{\mathrm{H}}_{\breve{\mathbf{u}}_{1,c_1}} \mathbf{\Phi}_{\breve{\mathbf{u}}_{1,c_1}})^{-1} \mathbf{\Phi}^{\mathrm{H}}_{\breve{\mathbf{u}}_{1,c_1}} \in \mathbb{C}^{K \times M}, \tag{3.8}$$

where $\mathbf{\Phi}_{\breve{\mathbf{u}}_{1,c_1}} \in \mathbb{C}^{M \times K}$ is a matrix made from the equivalent measurement matrix $\mathbf{\Phi}$ by choosing columns corresponding to $\breve{\mathbf{u}}_{i,c_1}$. With the aid of $\mathbf{\Phi}^{\dagger}_{\breve{\mathbf{u}}_{1,c_1}}$, the estimated SIM signal with $\breve{\mathbf{u}}_{1,c_1}$ can be represented by

$$\tilde{\mathbf{x}}_d(c_1) = \mathbf{\Phi}^{\dagger}_{\breve{\mathbf{u}}_{1,c_1}} \mathbf{y} \in \mathbb{C}^K. \tag{3.9}$$

For the estimated SIM signal, the following symbol-to-symbol ML detection for the k-th data symbol is carried out, which is expressed as

$$\tilde{q}(k,c_1) = \underset{q \in \mathcal{X}_{\mathrm{SIM}}}{\arg\min} |\tilde{x}_d(k,c_1) - q|^2 \quad (k = 0, ..., K-1), \tag{3.10}$$

Table 3.1: Simulation parameters in Fig. 3.2

M_{all}	256
N	15
M	8
K	2
Modulation	QPSK

where $|\cdot|^2$ denotes a squared absolute value and $\mathcal{X}_{\text{SIM}} \subset \mathbb{C}$ is a set of constellation points in SIM, e.g., QPSK. With the estimated symbols $\tilde{\mathbf{q}}(1), ..., \tilde{\mathbf{q}}(C_1)$, an estimated symbol set $\mathcal{X}_1 = \{\tilde{\mathbf{q}}(1), ..., \tilde{\mathbf{q}}(C_1)\} \subset \mathcal{X}_{\text{SIM}}^K$ is generated.

Finally, based on the index subset $\mathcal{I}_1$ and estimated symbol set $\mathcal{X}_1$, IRC detector calculates both estimated data symbol vector $\hat{\mathbf{x}}_d$ and index pattern $\hat{\mathbf{u}}$ by the following criterion

$$(\hat{\mathbf{x}}_d, \hat{\mathbf{u}}) = \underset{\breve{\mathbf{q}}(c_1)\in\mathcal{X}_1, \breve{\mathbf{u}}_{1,c_1}\in\mathcal{I}_1}{\arg\min} ||\mathbf{y} - \mathbf{\Phi}_{\breve{\mathbf{u}}_{1,c_1}} \breve{\mathbf{q}}||_2^2. \tag{3.11}$$

The above operations in (3.8)-(3.11) are iterated for the next index i_t until the iteration time t achieves a pre-defined maximum number $T \leq N$. Note that when T is set to N, operations in (3.8)-(3.11) included calculcation of Moore-Penrose pseudo-inverse matrix perform for all candidates of $\mathbf{x}$. Since the complexity order of calculating Moore-Penrose inverse matrix is cubic, IRC detector requires excessive complexity when more virtual subcarriers are activated to increase the transmission rate.

3.3 Performance evaluation

Firstly, we evaluate CS-SIM in terms of BER performance via computer simulation. Figure 3.2 shows the BER performances of CS-SIM and OFDM over frequency-selective Rayleigh fading channels where all the transmission rates are set as 1.25 bits/s/Hz. Simulation parameters are shown in Table 3.1. In OFDM, only 160 subcarriers are employed for data symbol transmission to set the same transmission rate to CS-SIM. As shown in Fig. 3.2, the BER performance of CS-SIM becomes better as increasing the number of iteration in IRC detector since the search space of IRC detector is expanded. Compared with the BER performance of OFDM, that of IRC detector is a significantly good performance.

3.4 Chapter conclusions

In this chapter, we introduced the conventional CS-SIM system employing IRC detector and showed that the BER performance of CS-SIM outperforms that of OFDM in terms of BER performance. However, IRC detector requires excessive complexity to obtain a

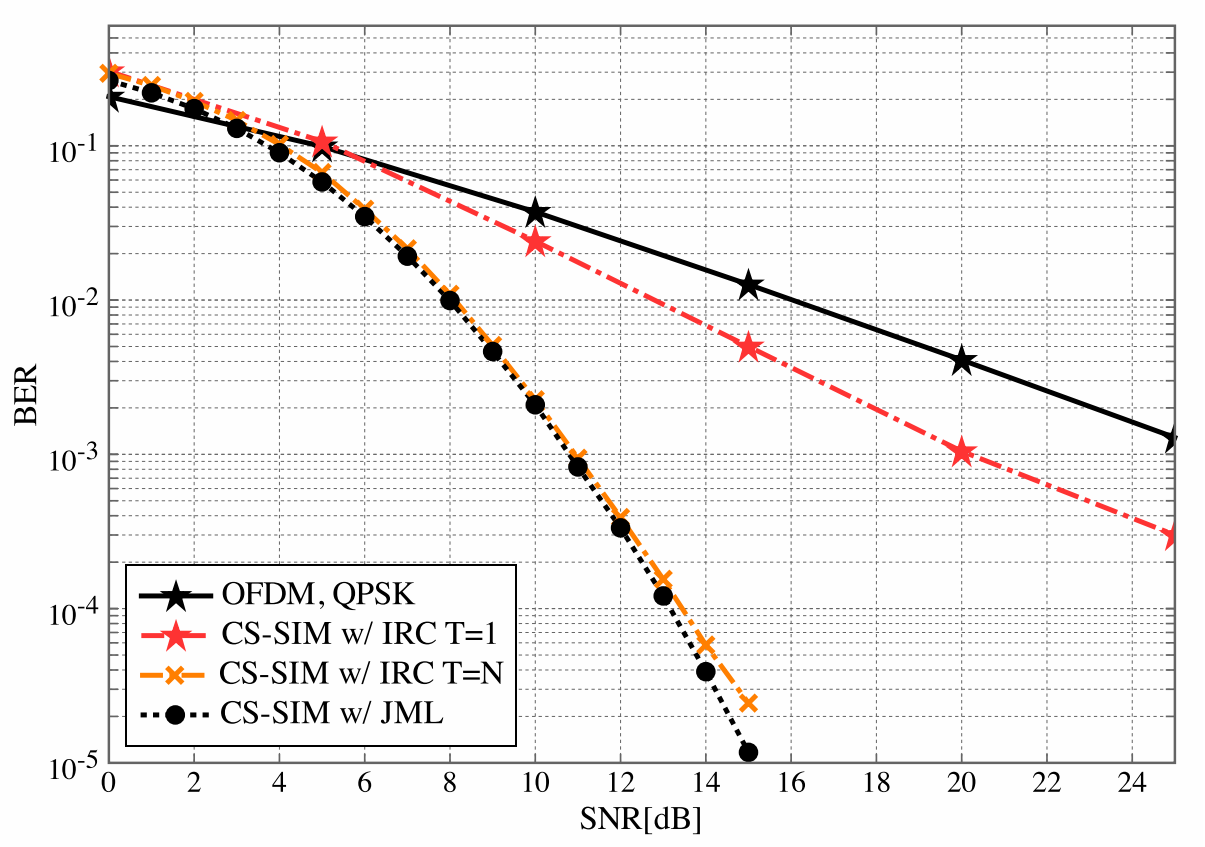

Figure 3.2: BER performance of CS-SIM and OFDM over frequency-selective Rayleigh fading channels where all the transmission rates are set as 1.25 bits/s/Hz.

good performance, so that the alternative of CS-SIM with low complexity and superiority over SIM and OFDM at higher transmission rate is required.

Chapter 4

Proposed CS-based SIQIM systems

In this chapter, we propose CS-SIQIM and AC-SIQIM systems. To increase the transmission rate, SIQIM, in which index patterns on in-phase and quadrature-phase can convey information bits, is employed in our proposal. Moreover, to lower the complexity, DFISTA, which requires square-order complexity, is employed. The detail of our proposal is as follows.

4.1 Proposed CS-SIQIM system

4.1.1 Transmitter

Our proposed CS-SIQIM system is shown in Fig. 4.1. We assume M_{all} subcarriers in every OFDM symbol and these subcarriers are divided into G subblocks, so that each subblock has $M = M_{\text{all}}/G$ subcarriers. Note that we assume N *virtual*-domain subcarriers per subblock, and the SIQIM signal is generated in the virtual domain, where $N > M$. In every subblock, the information-bit vector $\mathbf{p}_g \in \{0,1\}^B$, where $g = 1, 2, ..., G$ and B is the number of information bits conveyed by a subblock, is divided into two vectors $\mathbf{p}_g^{(\text{I})}, \mathbf{p}_g^{(\text{Q})} \in \{0,1\}^{B/2}$. Each vector is used to generate data symbol vectors $\mathbf{x}_{d,g}^{(\text{I})}, \mathbf{x}_{d,g}^{(\text{Q})} \in \mathcal{X}^K$ and index patterns $\mathbf{u}_g^{(\text{I})}, \mathbf{u}_g^{(\text{Q})} \in \mathcal{I}$ on in-phase and quadrature-phase in the virtual domain. To elaborate, $\mathcal{X} = \{\pm r_1, ..., \pm r_D\} \subset \mathbb{R}$ is supposed to be the pulse amplitude modulation (PAM) symbol set, and $r_1, ..., r_D$ are amplitudes of modulated signals where $r_1 < \ldots < r_D$, while $\mathcal{I}$ is the index set. When K out of N subcarriers are active, the number of subcarrier index patterns is given by $\Delta = \binom{N}{K}$. However, for carrying information bits, only $2^{\lfloor \log_2 \Delta \rfloor}$ patterns are employed. In this paper, all index patterns are constructed according to the combinatorial method of Basar [17, 18]. Then, only $2^{\lfloor \log_2 \Delta \rfloor}$ patterns are chosen in descending order. With the aid of $\mathbf{x}_{d,g}^{(\text{I})}$ and $\mathbf{u}_g^{(\text{I})}$, the virtual-domain SIM in-phase signal

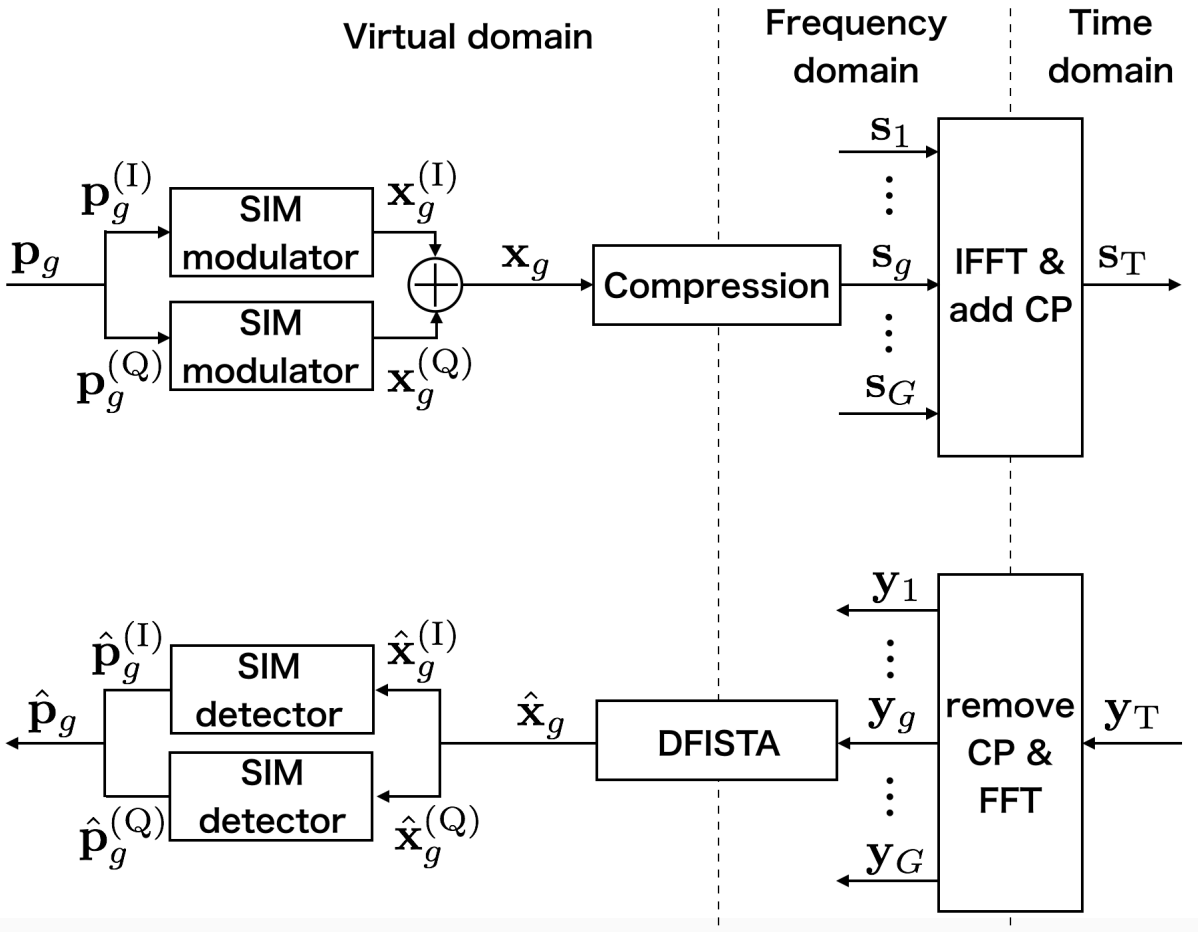

Figure 4.1: System model of CS-SIQIM with DFISTA.

is represented by

$$\mathbf{x}_g^{(\mathrm{I})} = \mathbf{I}_{\mathbf{u}_g^{(\mathrm{I})}} \mathbf{x}_{d,g}^{(\mathrm{I})} \tag{4.1}$$

$$= [0, ..., \underbrace{x_{d,g,1}^{(\mathrm{I})}}_{u_{g,1}^{(\mathrm{I})}\mathrm{th}}, ..., \underbrace{x_{d,g,2}^{(\mathrm{I})}}_{u_{g,2}^{(\mathrm{I})}\mathrm{th}}, ..., \underbrace{x_{d,g,K}^{(\mathrm{I})}}_{u_{g,K}^{(\mathrm{I})}\mathrm{th}}, ..., 0]^{\mathrm{T}} \in \mathbb{R}^N, \tag{4.2}$$

where $I_{\mathbf{u}_g^{(\mathrm{I})}} \in \{0,1\}^{N \times K}$ is a partial identity matrix constructed by choosing column vectors according to $\mathbf{u}_g^{(\mathrm{I})}$. Similar to the in-phase signal, the quadrature-phase signal $\mathbf{x}^{(\mathrm{Q})}$ is generated according to $\mathbf{x}_{d,g}^{(\mathrm{Q})}$ and $\mathbf{u}_g^{(\mathrm{Q})}$. Upon combining the two signals, the complex SIQIM signal is formulated as

$$\mathbf{x}_g = \mathbf{x}_g^{(\mathrm{I})} + j\mathbf{x}_g^{(\mathrm{Q})} \in \mathbb{C}^N. \tag{4.3}$$

Therefore, the number of information bits conveyed by a subblock is represented by

$$B = 2\left(K(1+\log_2 D) + \lfloor \log_2 \Delta \rfloor\right). \tag{4.4}$$

Then, the N-dimensional SIQIM signal is compressed into the M-dimensional signal $\mathbf{s}_g \in \mathbb{C}^M$, which is expressed as

$$\mathbf{s}_g = \mathbf{A}\mathbf{x}_g, \tag{4.5}$$

where $\mathbf{A} \in \mathbb{C}^{M\times N}$ denotes a measurement matrix and $\mathbb{E}[||\mathbf{s}_g||_2^2] = K$ holds for $g = 1, ..., G$. Figure 4.3 illustrates the compression of the virtual-domain signal $\mathbf{x}_g$ to the frequency-domain signal $\mathbf{s}_g$. According to [19], the restricted isometry property (RIP) as well as the null space property (NSP) and the mutual incoherence property (MIP) are influential in guaranteeing a high reconstruction performance. However, finding a measurement matrix to satisfy both the RIP and NSP is known to be an NP-hard problem [20]. By contrast, it is easier to verify that a specific measurement matrix satisfies the MIP than the RIP and NSP. Hence, we consider designing a measurement matrix which satisfies MIP. A mutual coherence of a measurement matrix $\mathbf{A}$ is defined as the largest absolute values amongst normalized inner products between different column vectors of $\mathbf{A}$, which is expressed as

$$\mu(\mathbf{A}) \triangleq \max_{0\le k<l\le N} \frac{|\mathbf{a}_k^{\mathrm{H}}\mathbf{a}_l|}{||\mathbf{a}_k||_2||\mathbf{a}_l||_2} \tag{4.6}$$

$$= \max_{0\le k<l\le N} \psi(\mathbf{A}, k, l), \tag{4.7}$$

where $\mathbf{a}_k$ and $\mathbf{a}_l$ are the k-th and l-th column vectors in $\mathbf{A}$, respectively. For the sake of simplicity, an inner product between the k-th and l-th column vectors in $\mathbf{A}$ is represented by $\psi(\mathbf{A}, k, l)$. To guarantee that there exists at most one signal $\mathbf{x}$ ensuring that $\mathbf{s} = \mathbf{A}\mathbf{x}$, the mutual coherence should be less than $1/(2K-1)$, while the lower bound of a mutual coherence is known as Welch-bound [15]. Therefore, the measurement matrix $\mathbf{A} \in \mathbb{C}^{M\times N}$ should satisfy the following inequality:

$$\sqrt{\frac{N-M}{M(N-1)}} \le \mu(\mathbf{A}) < \frac{1}{2K-1}. \tag{4.8}$$

If the mutual coherence of the measurement matrix is within the above inequality, the measurement matrix satisfies MIP. Here we have opted for designing the measurement matrix satisfying the MIP, which is constructed from N-point discrete Fourier transform (DFT) matrix by choosing rows to achieve the lower bound [7].

Compressed signals of all subblocks are gathered and combined into $\mathbf{s}_{\mathrm{F}} = [\mathbf{s}_1^{\mathrm{T}}, ..., \mathbf{s}_g^{\mathrm{T}}, ..., \mathbf{s}_G^{\mathrm{T}}]^{\mathrm{T}} \in \mathbb{C}^{M_{\mathrm{all}}}$. The frequency-domain compressed signal $\mathbf{s}_{\mathrm{F}}$ is converted into a time-domain signal by inverse fast Fourier transform (IFFT), and then, cyclic prefix (CP) is added to the resulted signal. CP added time-domain signal $\mathbf{s}_{\mathrm{T}}$ is transmitted.

4.1.2 Receiver

For the sake of simplicity, we assume communication over independent and identically distributed (i.i.d.) frequency-flat Rayleigh fading channels. This assumption is not unrealistic, because each subcarrier experiences approximately uncorrelated Rayleigh fading channels upon invoking the interleaved grouping method of [21]. Therefore, after removing the CP and FFT-based demodulation, the frequency-domain received signal $\mathbf{y}_F = [\mathbf{y}_1^{\mathrm{T}}, ..., \mathbf{y}_g^{\mathrm{T}}, ..., \mathbf{y}_G^{\mathrm{T}}]^{\mathrm{T}} \in \mathbb{C}^{M_{\mathrm{all}}}$ is obtained. Then, the frequency-domain received signal of the g-th subblock is expressed as

$$\mathbf{y}_g = \mathbf{H}_g \mathbf{s}_g + \mathbf{n}_g \tag{4.9}$$

$$= \mathbf{\Phi}_g \mathbf{x}_g + \mathbf{n}_g \in \mathbb{C}^M, \tag{4.10}$$

where $\mathbf{H}_g \in \mathbb{C}^{M \times M}$ is a diagonal channel matrix, whose diagonal elements obey $\mathcal{CN}(0, 1)$. Let $\mathbf{n}_g$ denote AWGN vector whose elements follow $\mathcal{CN}(0, N_0)$, where N_0 is the single-sided noise spectral density. Furthermore, $\mathbf{\Phi}_g = \mathbf{H}_g \mathbf{A} \in \mathbb{C}^{M \times N}$ is the g-th pseudo measurement matrix. For ease of later exposition, we also introduce the equivalent real-valued model of [22], where a real-valued received signal is represented by

$$\mathbf{y}_{g,\mathrm{r}} = \mathbf{\Phi}_{g,\mathrm{r}} \mathbf{x}_{g,\mathrm{r}} + \mathbf{n}_{g,\mathrm{r}} \in \mathbb{R}^{2M}, \tag{4.11}$$

where

$$\mathbf{y}_{g,\mathrm{r}} = [\Re\{\mathbf{y}_g^{\mathrm{T}}\}\ \Im\{\mathbf{y}_g^{\mathrm{T}}\}]^{\mathrm{T}} \in \mathbb{R}^{2M}, \tag{4.12}$$

$$\mathbf{\Phi}_{g,\mathrm{r}} = \begin{bmatrix} \Re\{\mathbf{\Phi}_g\} & -\Im\{\mathbf{\Phi}_g\} \\ \Im\{\mathbf{\Phi}_g\} & \Re\{\mathbf{\Phi}_g\} \end{bmatrix} \in \mathbb{R}^{2M \times 2N}, \tag{4.13}$$

$$\mathbf{x}_{g,\mathrm{r}} = [\Re\{\mathbf{x}_g^{\mathrm{T}}\}\ \Im\{\mathbf{x}_g^{\mathrm{T}}\}]^{\mathrm{T}} \in \mathbb{R}^{2N}, \tag{4.14}$$

$$\mathbf{n}_{g,\mathrm{r}} = [\Re\{\mathbf{n}_g^{\mathrm{T}}\}\ \Im\{\mathbf{n}_g^{\mathrm{T}}\}]^{\mathrm{T}} \in \mathbb{R}^{2M}. \tag{4.15}$$

As seen in (4.11) and Fig. 4.3, the system has to estimate $2N$ real-valued unknowns from $2M < 2N$ real-valued observations. This problem is circumvented by DFISTA upon exploiting both the sparsity and discrete nature of $\mathbf{x}_{g,\mathrm{r}}$, as detailed in Section 4.3.

4.2 Proposed AC-SIQIM system

We further propose AC-SIQIM to improve the reconstruction performance of DFISTA, where all SIQIM signals are jointly compressed via a measurement matrix. Therefore, the difference between CS-SIQIM and AC-SIQIM is the compression size. However, as predicted by (4.8), AC-SIQIM can allow Welch bound lowered via enlarging the compression size.

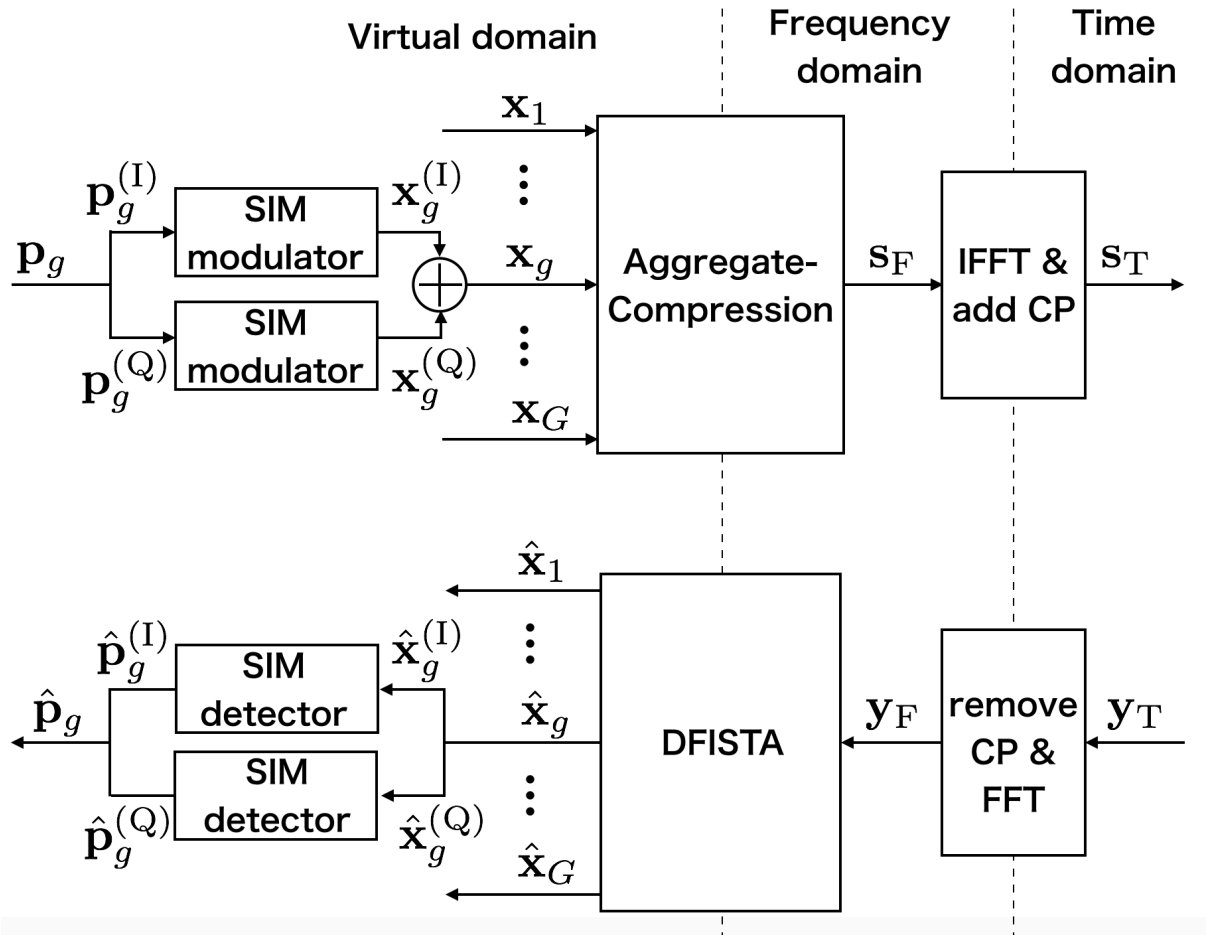

Figure 4.2: System model of AC-SIQIM with DFISTA.

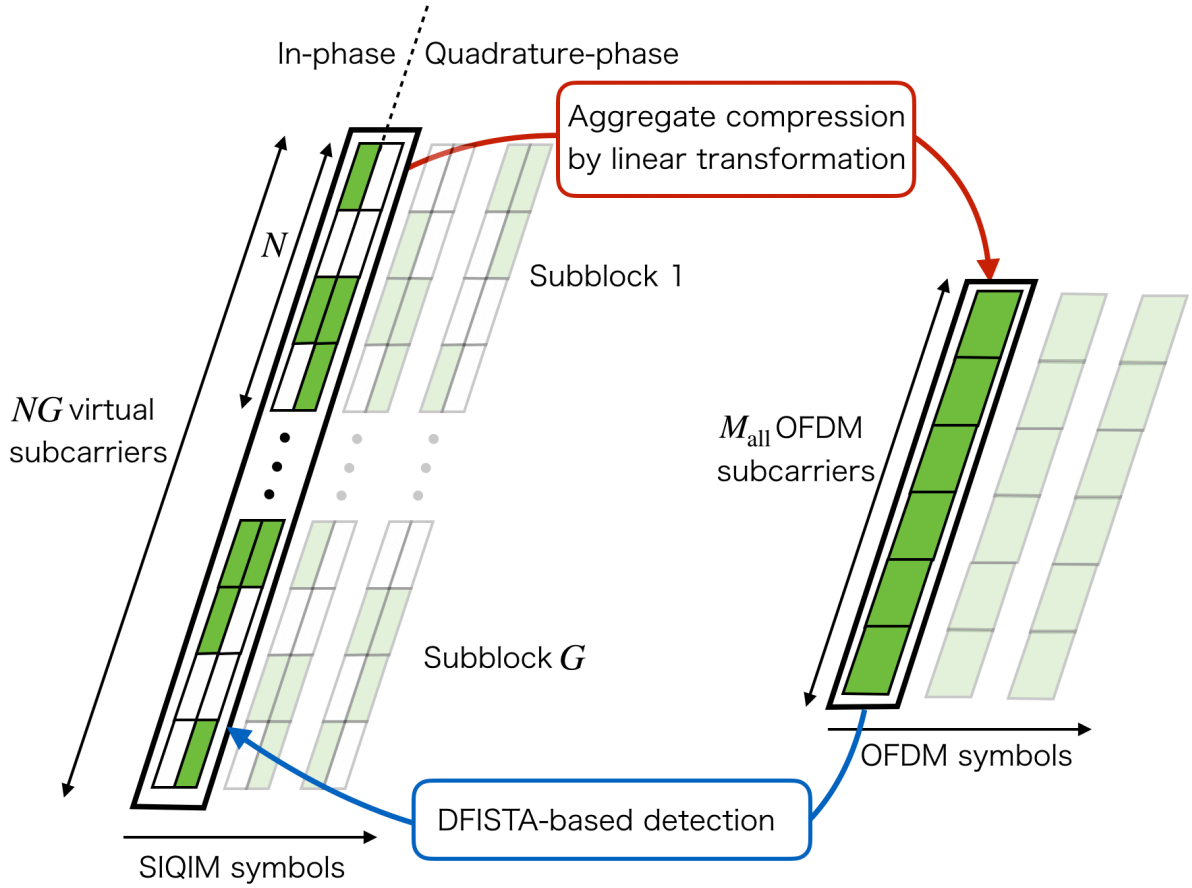

Figure 4.3: The compression of virtual-domain signal $\mathbf{x}$ to frequency-domain signal $\mathbf{s}$ and DFISTA-based detection of $\mathbf{x}$ from the received signal in AC-SIQIM where $NG > M_{\text{all}}$ holds, and the active index and the in-active index are represented by the dyed box and the blank box, respectively. A symbol in a virtual subcarrier consists of in-phase (left) and quadrature-phase (right) components.

4.2.1 Transmitter

Figure 4.2 shows the system model of AC-SIQIM with DFISTA. All SIQIM signals $\mathbf{x}_g$ are jointly compressed by a measurement matrix $\mathbf{A}_{\mathrm{AC}} \in \mathbb{C}^{M_{\mathrm{all}} \times NG}$, so that the compressed signal is expressed as

$$\mathbf{s}_{\mathrm{F}} = \mathbf{A}_{\mathrm{AC}}\mathbf{x} \in \mathbb{C}^{M_{\mathrm{all}}}, \tag{4.16}$$

where $\mathbf{x} = [\mathbf{x}_1^{\mathrm{T}}, ..., \mathbf{x}_g^{\mathrm{T}}, ..., \mathbf{x}_G^{\mathrm{T}}] \in \mathbb{C}^{NG}$. While the measurement matrix $\mathbf{A}$ for CS-SIM and CS-SIQIM is constructed from DFT matrix and designed to achieve Welch bound via an efficient construction method [23], it is hard to find such measurement matrix for a large size matrix even via the efficient method. Hence, for AC-SIQIM, we employ a complex Gaussian random matrix as a measurement matrix since its mutual coherence is sufficiently small when the matrix size is sufficiently large.

The compressed signal $\mathbf{s}$ is transformed into a time-domain signal via IFFT, and CP is added to the time-domain signal. The resulted signal $\mathbf{s}_{\mathrm{T}}$ is transmitted.

4.2.2 Receiver

We assume that wireless channels are i.i.d. frequency-flat Rayleigh fading as well, so that after the removal of CP and FFT, a frequency-domain received signal is expressed as

$$\mathbf{y}_{\mathrm{F}} = \mathbf{H}\mathbf{A}_{\mathrm{AC}}\mathbf{x} + \mathbf{n} \tag{4.17}$$

$$= \mathbf{\Phi}\mathbf{x} + \mathbf{n} \in \mathbb{C}^{M_{\mathrm{all}}}, \tag{4.18}$$

where $\mathbf{H} \in \mathbb{C}^{M_{\mathrm{all}} \times M_{\mathrm{all}}}$ is a diagonal channel matrix whose diagonal elements obey $\mathcal{CN}(0, 1)$ and $\mathbf{n}$ is AWGN vector whose elements follow $\mathcal{CN}(0, N_0)$. In contrast to CS-SIQIM, in AC-SIQIM, all SIQIM signals are jointly estimated from the received signal $\mathbf{y}_{\mathrm{F}}$ through DFISTA.

4.3 Proposed detector based on DFISTA

In this section, DFISTA is first introduced and detailed, then the detector based on DFISTA for the proposed CS-SIQIM and AC-SIQIM is described. To enhance the performance of the proposed detector, the efficient optimization method for hyperparameters of DFISTA is proposed. Furthermore, the detector complexities are evaluated to show the advantage of our proposed.

4.3.1 Discreteness-Aware FISTA

Without loss of generality, in the following, we omit the subblock index g. We consider estimating a higher-dimensional SIQIM signal from a lower-dimensional received signal, which is known as an underdetermined system. In CS, the specific characteristics of the estimate, such as its sparsity are exploited for estimation. Classically, the optimization problem conceived for finding the sparse solution has relied on the l_0 norm. However, the l_0 optimization is NP-hard. Therefore, instead of the l_0 norm, the l_1 norm is used to find our sparse solution. When the measurements constituted by the received signals in our scenario are contaminated by noise, $l_1 - l_2$ optimization is considered, which is expressed as

$$\min_{\mathbf{x}_\mathrm{r}} \left(f(\mathbf{x}_\mathrm{r}) + q_0 ||\mathbf{x}_\mathrm{r}||_1 \right), \tag{4.19}$$

where $f(\mathbf{x}_\mathrm{r}) = 0.5||\mathbf{\Phi}_\mathrm{r}\mathbf{x}_\mathrm{r} - \mathbf{y}_\mathrm{r}||_2^2$. FISTA is known as an efficient algorithm of solving the $l_1 - l_2$ optimization problem by exploiting a previous solution. However, FISTA exploits only the sparsity of the original signals $\mathbf{x}_\mathrm{r}$. If $\mathbf{x}_\mathrm{r}$ is discrete, this additional constraint can also be exploited to estimate them more efficiently with the aid of the so-called SOAV optimization [9, 11]. Bearing this in mind, the above optimization is rewritten as

$$\min_{\mathbf{x}_\mathrm{r}} \left(f(\mathbf{x}_\mathrm{r}) + q_0 ||\mathbf{x}_\mathrm{r}||_1 + \sum_{l=1}^{D} q_l \left(||\mathbf{x}_\mathrm{r} - r_l \mathbf{1}||_1 + ||\mathbf{x}_\mathrm{r} + r_l \mathbf{1}||_1 \right) \right), \tag{4.20}$$

where q_l $(l = 0, 1, ..., D)$ are hyper-parameters, which control the balance amongst terms. Then, $f(\mathbf{x}_\mathrm{r})$ is from a closed convex subset $\mathcal{C}$ of the $2N$ dimensional Euclidean space $\mathbb{R}^{2N}$.

For later discussion, we assume that the function $f(\mathbf{x}_\mathrm{r})$ is differentiable and its gradient $\nabla f(\mathbf{x}_\mathrm{r})$ is Lipshitz, which means that there exists a Lipshitz constant L for any $\mathbf{x}_\mathrm{r}, \mathbf{v}_\mathrm{r} \in \mathcal{C}$,

$$||\nabla f(\mathbf{x}_\mathrm{r}) - \nabla f(\mathbf{v}_\mathrm{r})||_2 \leq L ||\mathbf{x}_\mathrm{r} - \mathbf{v}_\mathrm{r}||_2. \tag{4.21}$$

To solve (4.20), we define a quadratic approximation model of $f(\mathbf{x}_\mathrm{r})$ at given point $\mathbf{v}_\mathrm{r}$:

$$q_L(\mathbf{x}_\mathrm{r}, v_\mathrm{r}) := f(\mathbf{v}_\mathrm{r}) + \nabla f(\mathbf{v}_\mathrm{r})^\mathrm{T} (\mathbf{x}_\mathrm{r} - \mathbf{v}_\mathrm{r}) + \frac{L}{2} ||\mathbf{x}_\mathrm{r} - \mathbf{v}_\mathrm{r}||_2^2. \tag{4.22}$$

Algorithm 1 DFISTA

Require: $\mathbf{y}_\mathrm{r} \in \mathbb{R}^{2M}$ (observed vector)
Ensure: $\hat{\mathbf{x}}_\mathrm{r} \in \mathbb{R}^{2N}$ (estimated vector)
1: $\mathbf{x}_\mathrm{r}[0] := \mathbf{\Phi}_\mathrm{r}^\mathrm{T}\mathbf{y}_\mathrm{r}$
2: $\mathbf{w}_\mathrm{r}[1] := \mathbf{x}_\mathrm{r}[0]$
3: $\beta[1] = 1$
4: $\sigma^2[0] = ||\mathbf{x}[0] - \mathcal{R}(\mathbf{x}[0])||_2^2/2N$
5: $k = 1$
6: **repeat**
7: $\quad \mathbf{x}_\mathrm{r}[k] := \eta(\mathbf{w}_\mathrm{r}[k] - L^{-1}\mathbf{\Phi}_\mathrm{r}^\mathrm{T}(\mathbf{y}_\mathrm{r} - \mathbf{\Phi}_\mathrm{r}\mathbf{w}_\mathrm{r}[k]), \sigma)$
8: $\quad \beta[k+1] := \frac{1}{2} + \sqrt{\frac{1}{4} + \beta[k]^2}$
9: $\quad \mathbf{w}_\mathrm{r}[k+1] := \mathbf{x}_\mathrm{r}[k] + \frac{\beta[k]-1}{\beta[k+1]}(\mathbf{x}_\mathrm{r}[k] - \mathbf{x}_\mathrm{r}[k-1])$
10: $\quad \sigma^2[k] = ||\mathbf{x}_\mathrm{r}[k] - \mathcal{R}(\mathbf{x}_\mathbf{r}[k])||_2^2/2N$
11: $\quad k := k + 1$
12: **until** $k = T_\mathrm{max}$
13: **return** $\hat{\mathbf{x}}_\mathrm{r} := \mathbf{x}_\mathrm{r}[k-1]$

If (4.21) holds, we obtain the following inequality $f(\mathbf{x}_\mathrm{r}) \leq q_L(\mathbf{x}_\mathrm{r}, \mathbf{v}_\mathrm{r})$. This technique is known as the majorization-minimization (MM) approach [24], and $q_L(\mathbf{x}_\mathrm{r}, \mathbf{v}_\mathrm{r})$ is referred to as a majorizer of the function $f(\mathbf{x}_\mathrm{r})$. Upon applying the MM approach to $f(\mathbf{x}_\mathrm{r})$ in (17), we obtain

$$\begin{aligned} Q_L(\mathbf{x}_\mathrm{r}, \mathbf{v}_\mathrm{r}) = &\frac{1}{2}||\mathbf{\Phi}_\mathrm{r}\mathbf{v}_\mathrm{r} - \mathbf{y}_\mathrm{r}||_2^2 + (\mathbf{x}_\mathrm{r} - \mathbf{v}_\mathrm{r})^\mathrm{T}\mathbf{\Phi}_\mathrm{r}^\mathrm{T}(\mathbf{\Phi}_\mathrm{r}\mathbf{x}_\mathrm{r} - \mathbf{y}_\mathrm{r}) \\ &+ \frac{L}{2}||\mathbf{x}_\mathrm{r} - \mathbf{v}_\mathrm{r}||_2^2 + q_0||\mathbf{x}_\mathrm{r}||_1 + \sum_{l=1}^{D} q_l \left(||\mathbf{x}_\mathrm{r} - r_l\mathbf{1}||_1 + ||\mathbf{x}_\mathrm{r} + r_l\mathbf{1}||_1\right) \\ = &\frac{L}{2}||\mathbf{x}_\mathrm{r} - (\mathbf{v_r} - L^{-1}\mathbf{\Phi}_\mathrm{r}^\mathrm{T}(\mathbf{\Phi}_\mathrm{r}\mathbf{v}_\mathrm{r} - \mathbf{y}_\mathrm{r}))||_2^2 - \frac{L}{2}||\mathbf{\Phi}_\mathrm{r}^\mathrm{T}(\mathbf{\Phi}_\mathrm{r}\mathbf{v_r} - \mathbf{y_r})||_2^2 + q_0||\mathbf{x}_\mathrm{r}||_1 \\ &+ \sum_{l=1}^{D} q_l \left(||\mathbf{x}_\mathrm{r} - r_l\mathbf{1}||_1 + ||\mathbf{x}_\mathrm{r} + r_l\mathbf{1}||_1\right) + \frac{1}{2}||\mathbf{\Phi}_\mathrm{r}\mathbf{v}_\mathrm{r} - \mathbf{y}_\mathrm{r}||_2^2. \end{aligned} \tag{4.23}$$

Eliminating the constant terms from the above equation, the above equation can be rewritten as

$$\begin{aligned} Q_L(\mathbf{x}_\mathrm{r}, \mathbf{v}_\mathrm{r}) = &\frac{L}{2}||\mathbf{x}_\mathrm{r} - (\mathbf{v}_\mathrm{r} - L^{-1}\mathbf{\Phi}_\mathrm{r}^\mathrm{T}(\mathbf{\Phi}_\mathrm{r}\mathbf{v}_\mathrm{r} - \mathbf{y}_\mathrm{r}))||_2^2 \\ &+ q_0||\mathbf{x}_\mathrm{r}||_1 + \sum_{l=1}^{D} q_l \left(||\mathbf{x}_\mathrm{r} - r_l\mathbf{1}||_1 + ||\mathbf{x}_\mathrm{r} + r_l\mathbf{1}||_1\right). \end{aligned} \tag{4.24}$$

According to the basic concept of minimizing the above equation, we define the iterative

equation:

$$\begin{aligned}
&\mathbf{x}_{\mathrm{r}}[k+1] \\
&= \arg\min_{\mathbf{x}_{\mathrm{r}}} Q_L(\mathbf{x}_{\mathrm{r}}, \mathbf{x}_{\mathrm{r}}[k]) \\
&= \arg\min_{\mathbf{x}_{\mathrm{r}}} \left(\frac{L}{2} ||\mathbf{x}_{\mathrm{r}} - \boldsymbol{\phi}(\mathbf{x}_{\mathrm{r}}[k])||_2^2 + q_0 ||\mathbf{x}_{\mathrm{r}}||_1 + \sum_{l=1}^{D} q_l (||\mathbf{x}_{\mathrm{r}} - r_l \mathbf{1}||_1 + ||\mathbf{x}_{\mathrm{r}} + r_l \mathbf{1}||_1) \right), \quad (4.25)
\end{aligned}$$

where $\boldsymbol{\phi}(\mathbf{x}_{\mathrm{r}}) = \mathbf{x}_{\mathrm{r}} - L^{-1}\boldsymbol{\Phi}_{\mathrm{r}}^{\mathrm{T}}(\boldsymbol{\Phi}_{\mathrm{r}}\mathbf{x}_{\mathrm{r}} - \mathbf{y}_{\mathrm{r}})$. The solution of the optimization problem can be found by minimizing each element independently. According to [9, 25], the minimizer of the objective function given by (4.20) is the following soft thresholding function.

$$[\eta(\mathbf{v}), \sigma]_i = \begin{cases}
v_i + U_D\sigma & (v_i < -r_D - U_D\sigma) \\
\vdots & \\
-r_l & (-r_l - U_l\sigma \le v_i < -r_l - U_{l-1}\sigma) \\
v_i + U_{l-1}\sigma & (-r_l - U_{l-1}\sigma \le v_i < -r_{l-1} - U_{l-1}\sigma) \\
\vdots & \\
0 & (-U_0\sigma \le v_i < U_0\sigma) \\
\vdots & \\
v_i - U_{l-1}\sigma & (r_{l-1} + U_{l-1}\sigma \le v_i < r_l + U_{l-1}\sigma) \\
r_l & (r_l + U_{l-1}\sigma \le v_j < r_l + U_l\sigma) \\
\vdots & \\
v_j - U_D\sigma & (r_D + U_D\sigma \le v_j)
\end{cases}, \quad (4.26)$$

where U_l $(l = 1, ..., D)$ are positive hyper parameters, and $\sigma^2[k]$ is the residual MSE of the k-th estimate. An example of soft thresholding function is illustrated in Fig. 4.4. Since DFISTA is based on original FISTA [13], the DFISTA technique can be summarized as Algorithm 1, where L is the Lipschitz constant of $f(\mathbf{x}_{\mathrm{r}})$ while $\beta[k+1]$ and $\mathbf{w}[k+1]$ are introduced to accelerate the convergence. Furthermore, $\mathcal{R}(\mathbf{v})$ is a mapping function, which maps each element of $\mathbf{v}$ to the closest signal point in $\mathcal{X}$.

4.3.2 Detection of the SIQIM signal

Based on the aforementioned DFISTA, our detector for SIQIM signals is described here. An equivalent real-valued model defined by (4.11) is assumed, since the in-phase and quadrature-phase components are independent in CS-SIQIM. Instead of directly estimating the information bits in the received compressed signals $\mathbf{y}_{\mathrm{r}}$, the virtual received signals $\hat{\mathbf{x}}_{\mathrm{r}}$ are reconstructed firstly from $\mathbf{y}_{\mathrm{r}}$ through DFISTA. Once $\hat{\mathbf{x}}_{\mathrm{r}}$ is obtained, we can use

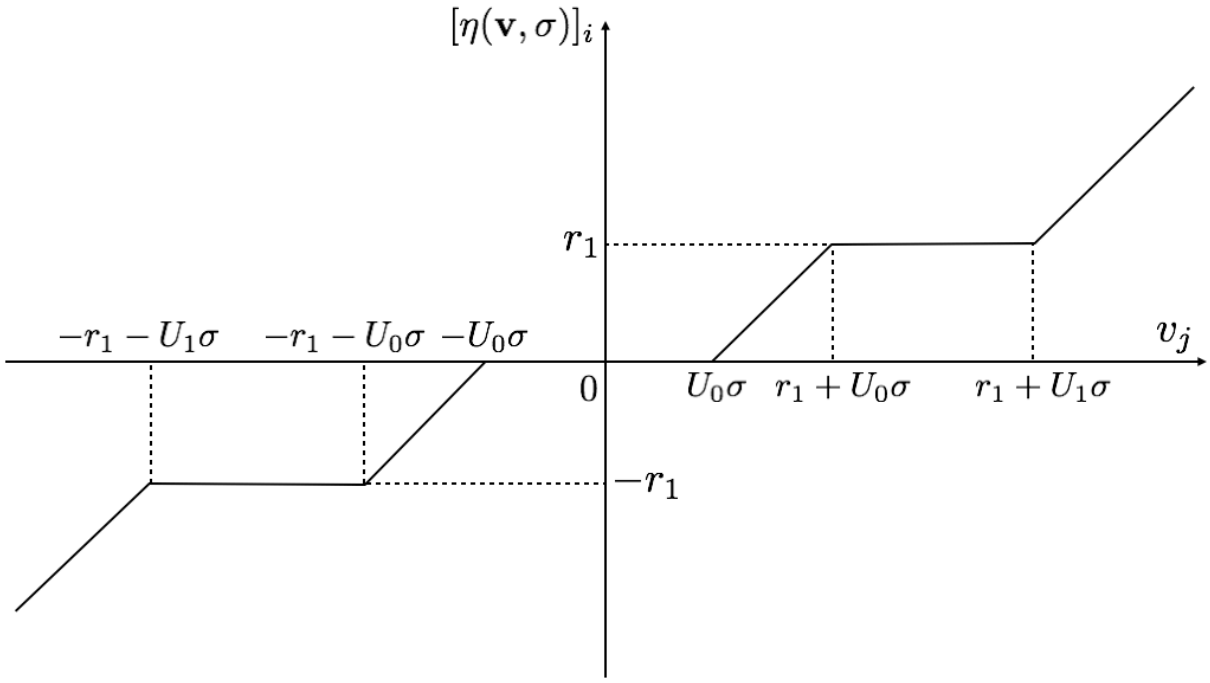

Figure 4.4: Soft thresholding function with $D = 1$. Hyperparameters U_l control the range of linear and constant.

the conventional JML detector for SIM [17, 18]. Specifically, for the in-phase signal, we have

$$\hat{\mathbf{p}}^{(\mathrm{I})} = \Psi(\hat{\mathbf{x}}_d^{(\mathrm{I})}, \hat{\mathbf{u}}^{(\mathrm{I})}) = \Psi\left(\underset{\mathbf{v}\in\mathcal{X}^K, \mathbf{z}\in\mathcal{I}}{\arg\min} ||\hat{\mathbf{x}}^{(\mathrm{I})} - \mathbf{I}_{\mathbf{z}}\mathbf{v}||_2^2\right), \tag{4.27}$$

where Ψ is a mapping function, which jointly maps data symbols and an index to the corresponding bit vector. Similar to the in-phase signal, the quadrature-phase signal is detected by JML detection.

4.3.3 Optimization of hyperparameters based on differential evolution

Hyperparameters U_l play an important role of balancing evaluations of Euclidean distance, sparseness, and discreteness, so that hyperparameters significantly affect the reconstruction performance of DFISTA. If hyperparameters in DFISTA are optimized in terms of minimizing the MSE, DFISTA does not necessarily exhibit the lowest BER since DFISTA-based detector consists of not only DFISTA but also SIQIM detection in (4.27). Also, there is no optimization method for hyperparameters in an algorithm based on FISTA. While the hyperparameters are determined with prior probabilities of discrete

values in [25], these hyperparameters should be optimized for each SNR since the balance among $l_1 - l_2$ norms obviously depends on SNR. Moreover, more hyperparameters have to be optimized upon increasing the order of modulation. Hence, we further propose an efficient optimization method based on DE [16]

Hereafter, the vector notation $\mathbf{u}_{\mathrm{DFISTA}} = [U_0, ..., U_D]^{\mathrm{T}} \in \mathbb{R}_+^{D+1}$ is used where $\mathbb{R}_+$ denotes positive real. The vector is optimized to minimize the BER performances of CS-SIQIM and AC-SIQIM. At first, P vectors are randomly generated as

$$\boldsymbol{\gamma}_{i,0} = [\gamma_{i,0,0}, ..., \gamma_{i,0,D}]^{\mathrm{T}} \ (i = 1, ..., P), \tag{4.28}$$

where

$$\gamma_{i,0,l} = \gamma_{l,\min} + \mathrm{rand}[0, 1] \cdot (\gamma_{l,\max} - \gamma_{l,\min}), \tag{4.29}$$

for $l = 0, ..., D$, $\gamma_{l,\max}$ and $\gamma_{l,\min}$ are maximum and minimum values of U_l, respectively. These generated vectors are candidates of $\mathbf{u}_{\mathrm{DFISTA}}$. To obtain the diversity among these random vectors, three vectors which are randomly chosen are mixed into one vector, which is expressed as

$$\boldsymbol{\zeta}_{i,o} = \boldsymbol{\gamma}_{c_1,o} + F \cdot (\boldsymbol{\gamma}_{c_2,o} - \boldsymbol{\gamma}_{c_3,o}), \tag{4.30}$$

for the o-th iteration where F is a scaling factor which controls a trade-off between divergence and convergence, and c_1, c_2, c_3 are indices chosen randomly from $\{1, ..., P\}$, respectively.

In the next step, a partial permutations of $\boldsymbol{\gamma}_{i,o}$ and $\boldsymbol{\zeta}_{i,o}$ is performed to diverge candidates. Let $\alpha, \beta \in \{0, ..., D\}$ denote the starting index of the permutation and the number of permuted parameters, respectively. Given α and β, a parameter of a permuted vector is represented by

$$\xi_{i,o,l} = \begin{cases} \zeta_{i,o,l} & \text{for } i = \alpha(\mathrm{mod}\ D), ..., \alpha + \beta(\mathrm{mod}\ D) \\ \gamma_{i,o,l} & \text{otherwise} \end{cases}, \tag{4.31}$$

for $l = 0, ..., D$.

Finally, comparing $\boldsymbol{\gamma}_{i,o}$ and $\boldsymbol{\xi}_{i,o}$ in terms of BER, new parameter-vectors are generated, which is expressed as

$$\boldsymbol{\gamma}_{i,o+1} = \begin{cases} \boldsymbol{\gamma}_{i,o} & \text{if } \mathrm{BER}(\boldsymbol{\gamma}_{i,o}) \leq \mathrm{BER}(\boldsymbol{\xi}_{i,o}) \\ \boldsymbol{\xi}_{i,o} & \text{otherwise} \end{cases}, \tag{4.32}$$

where $\mathrm{BER}(\boldsymbol{\gamma})$ denotes the BER performance fo the CS-SIQIM and AC-SIQIM when $\boldsymbol{\gamma}$ is used as hyperparameters. Oprations defined by (4.30)-(4.32) are performed iteratively until the difference between the o-th and the $(o+1)$-th generations' BERs is sufficiently small.

4.4 Chapter conclusions

In this chapter, we proposed CS-SIQIM and AC-SIQIM system and optimization method for hyperparameters in DFISTA. By employing SIQIM, the transmission rate is significantly increased. Moreover, to improve the reconstruction performance of DFISTA, we proposed the joint compression of SIQIM signals, named AC. In the next section, our proposals are evaluated in terms of BER performance and complexity by comparing with OFDM and SIM, and the conventional CS-SIM.

Chapter 5

Numerical Results

5.1 Complexity comparison of DFISTA-based, IRC, and JML detectors

The computational complexity of DFISTA is analyzed by comparing it with the conventional detectors: JML detector and IRC detector. For a fair comparison, complexities of these detectors per subblock are evaluated. In addition, it is known that multiplication is dominant in computational complexity, so that the number of real-valued multiplications is investigated, which is summarized in Table 5.1 where $M \triangleq M_{\text{all}}/G$.

(1) JML detector

The number of all candidates of SIM is $(2D)^K \cdot 2^{\lfloor \log_2 \binom{N}{K} \rfloor}$. For each candidate, two matrix-vector multiplications are required, so that the number of real-valued multiplications for one candidate is $4KNM$.

(2) IRC detector

MMSE estimation requires $(4N^3 + 8N^2M)$ multiplications. To achieve the best performance of IRC detector, N iterations are needed. Therefore, IRC detector has to search a solution from all the index patterns in $\mathcal{I}$ whose number is $2^{\lfloor \log_2 \binom{N}{K} \rfloor}$. For each candidate, Moore-Penrose pseudo-inverse matrix and one matrix-vector product are calculated, so that $(12K^2M + 4K^3 + 8DK)$ real-valued multiplication are required.

(3) DFISTA-based detector

The algorithm of DFISTA-based detector is divided into two parts: DFISTA and JML detection. In the DFISTA part, $4M_{\text{all}}NG$ real-valued multiplication is required for the first estimation $\mathbf{x}[0]$. At each iteration, two matrix-vector products are required, so that the number of real-valued multiplications is $8M_{\text{all}}NG$. Therefore, DFISTA part requires

Table 5.1: The number of multiplications in IRC detector, and DFISTA-based detector.

	The number of real-valued multiplications
JML detector	$4KNM(2D)^K 2^{\lfloor \log_2 \binom{N}{K} \rfloor}$
IRC detector [7]	$4N^3 + 8N^2M + 2^{\lfloor \log_2 \binom{N}{K} \rfloor} \cdot (12K^2M + 4K^3 + 8DK)$
DFISTA-based detector	$4MN + T_{\max} \cdot (8MN + 2N + 1)$

$(4M_{\text{all}}NG + 8M_{\text{all}}NGT_{\max})$. Since the reconstructed vector $\hat{\mathbf{x}}$ does not contain any channel effect, JML detection shown in (4.27) does not require any multiplications. Note that, for fair comparison, the resulting number of multiplications is divided by the number of subblocks G.

Figure 5.1 shows the computational complexities per subblock of DFISTA-based, JML, IRC detectors where $N = 31, M = 16, D = 1, m = 5$, and $T_{\max} = 100$. Obviously, while the computational complexities of IRC and JML detectors increase with the number of active subcarriers K, that of DFISTA-based detector is independent of K. In addition, compared with the complexity of IRC detector, that of our proposal has lower complexity with $K > 2$. From the figure, DFISTA-based detector is applicable for CS-SIQIM system with high transmission rates since the complexity of the detector is constant even as increasing the number of active subcarriers.

5.2 Effect of aggregate-compression on mutual coherence

Figure 5.2 shows Welch bounds and cumulative density functions (CDFs) of several sizes of complex Gaussian random matrices. In conventional CS-SIM [7], 16×31-element matrix whose mutual coherence achieves Welch bound is employed. If a mutual coherence of a matrix achieves Welch bound, all coherences $\psi(\mathbf{A}, k, l)$ are identical. Hence, the behavior of the CDF is similar to the step function as shown in Fig. 5.2. On the other hand, CDFs of complex Gaussian random matrices whose sizes are 256×496 and 512×992 are distributed around corresponding Welch bounds. Comparing 256×496 and 512×992, the larger matrix has more column vectors whose coherence is smaller than Welch bound. Thanks to this lower coherence property, the larger random matrix provides better BER compared with the 16×31 constructed matrix which achieves Welch bound.

5.3 Comparison of BER performances

The BER performance of CS-SIQIM and AC-SIQIM using DFISTA is evaluated by comparing with OFDM and SIM, and CS-SIM using JML, IRC detector. Simulation param-

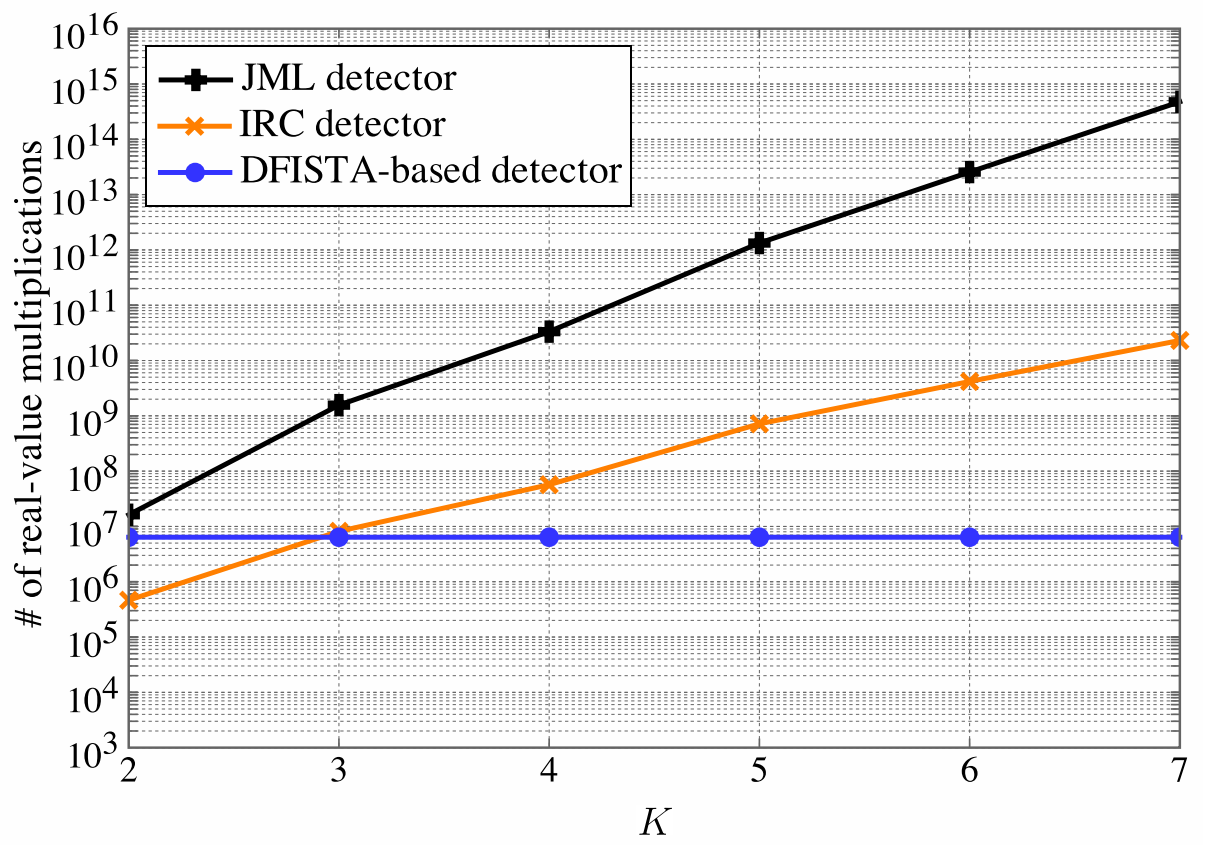

Figure 5.1: The numbers real-valued multiplications in DFISTA-based, IRC, JML detectors where $N = 15, M = 8, D = 1, T = N$ (in IRC), $T_{\max} = 50$ (in DFISTA).

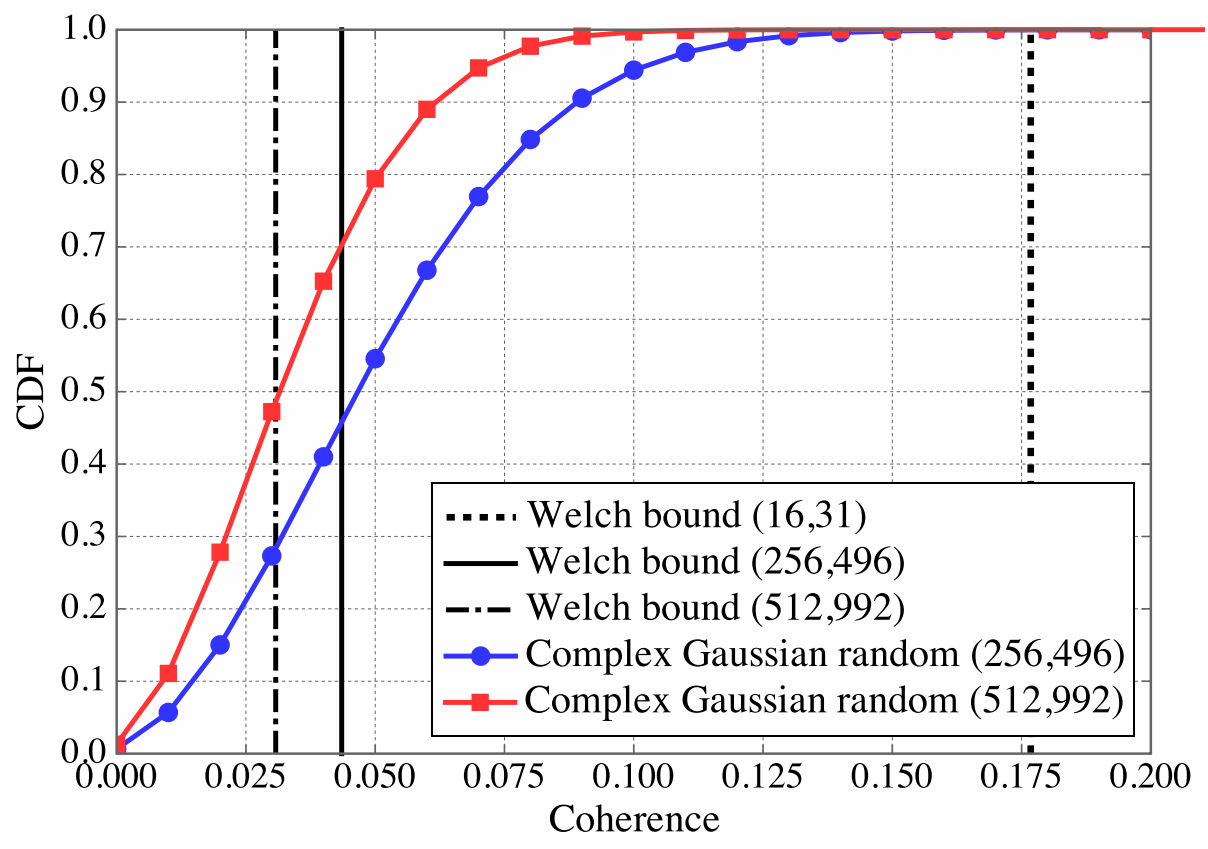

Figure 5.2: Welch bounds and cumulative density functions of several sizes of complex Gaussian random matrices.

Table 5.2: Simulation parameters in Fig. 5.3-5.5. Parameters used in a result is shown by notation in the figures, e.g., 'CS-SIM(15,8,2)'

	CS-SIM w/ IRC detector	CS-SIQIM w/ DFISTA	AC-SIQIM w/ DFISTA
M_{all}	256		256, 512
G	16		16,32
M	8	16	-
N	15	31	
K	2	2	2,3
D	-	1	1,2,4

eters used are shown in Table 5.2. The Lipschitz constant is set to $L = 2||\mathbf{\Phi}^T\mathbf{\Phi}||_2$ [26]. Complex Gaussian random matrix is employed as the measurement matrix $\mathbf{A}_{\text{AC}}$ in AC-SIQIM systems. In CS-SIM and CS-SIQIM, a partial DFT matrix whose mutual coherence achieves Welch bound. Hyperparameters $U_0, .., U_D$ are optimized to minimize the BER performance via DE descrived in Section 4.3.3. SNR per symbol and E_b/N_0 are defined as $\mathbb{E}[||\mathbf{s}||_2^2]/\mathbb{E}[||\mathbf{n}||^2] = K/MN_0$ and K/BMN_0, respectively, where E_b denote signal power per information bit. In this section, we use the notation "CS-SIM(N, M, K)," which represents every subblock of CS-SIM having a total of N virtual subcarriers, M OFDM subcarriers, and K active subcarriers. Moreover, for CS-SIQIM and AC-SIQIM, we also use the notation "CS-SIQIM(N, M, K)" and "AC-SIQIM(NG, M_{all}, K)". "CS-SIQIM(N, M, K)" represents K out of N virtual subcarriers are activated in each in-phase and quadrature-phase and the SIQIM signal is compressed into a M-dimensional signal. "AC-SIQIM(NG, M_{all}, K)" represents G SIQIM signals, which are N-dimensional vectors and have K nonzero elements on each in-phase and quadrature-phase, are jointly compressed into a M_{all}-dimensional OFDM signal.

Figure 5.3 shows the BER performance of CS-SIM using the IRC detector and of CS/AC-SIQIM relying on DFISTA-based detector for transmission over Rayleigh fading channels, where the number of IRC iterations is set to $T = 1$ or N(maximum) while the numbers of iterations in DFISTA is set to 100. The figure indicates that the BER of CS-SIM using the IRC detector is improved by increasing the number of iterations T. Our proposed AC-SIQIM with DFISTA outperforms CS-SIM with IRC detector at high SNR region and obtains about 2 dB gain against CS-SIM with IRC detector at BER= 10^{-5}.

Since our original motivation is to improve the bandwidth efficiency of SIM, the BER performance of CS/AC-SIQIM is evaluated at a higher transmission rate. In Fig. 5.4, our proposed CS/AC-SIQIM using DFISTA is compared with conventional OFDM and SIM where the transmission rates of CS/AC-SIQIM with DFISTA and OFDM are set to 1.875 bits/s/Hz while that of SIM is set to 1.75 bits/s/Hz. In the conventional OFDM and SIM, QPSK is employed, while in our scheme 2-PAM is employed on each in-phase

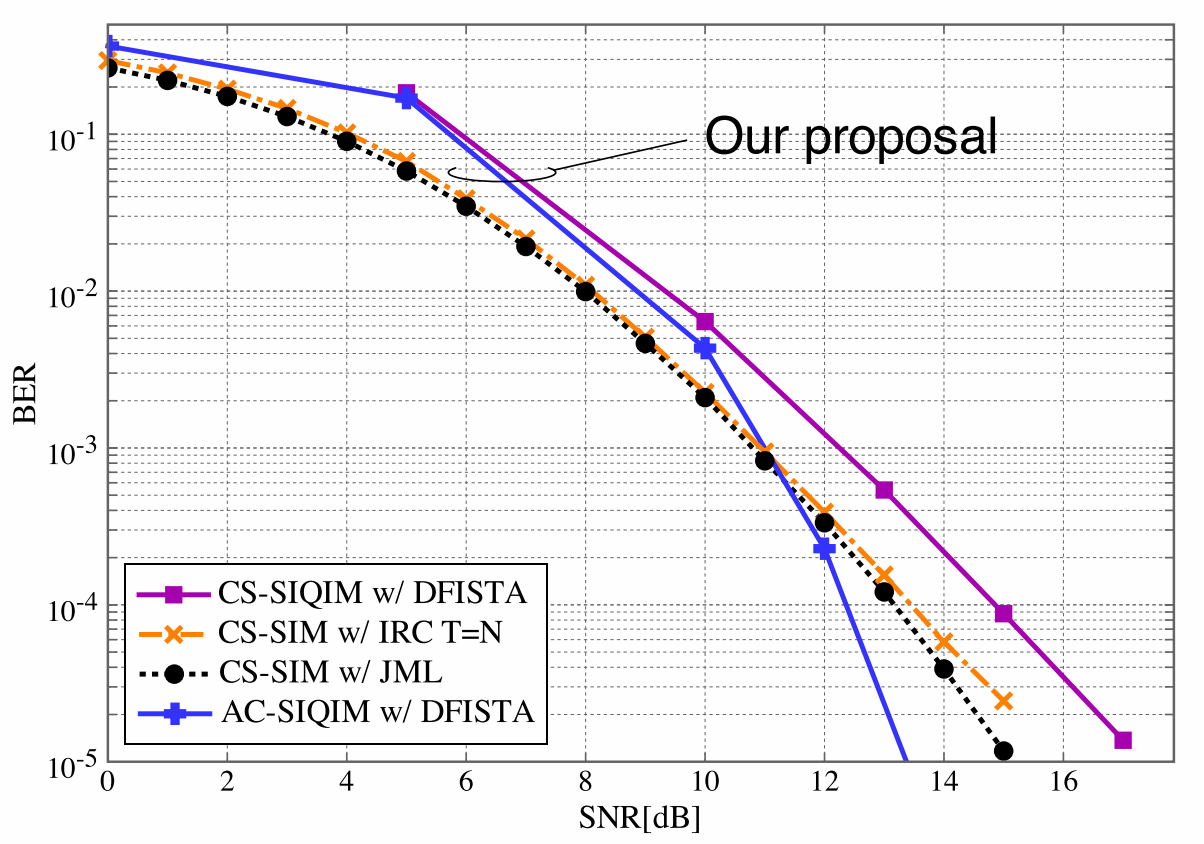

Figure 5.3: BER performance of CS-SIM with IRC detector and of CS/AC-SIQIM with DFISTA-based detector where the transmission rates are set as 1.25 bit/s/Hz. The number of iteration in IRC detector is $T = 1, N$. The number of iteration in DFISTA is 100.

and quadrature-phase. Moreover, only 240 subcarriers out of $M_{\text{all}} = 256$ subcarriers are used for data symbol transmission in OFDM to adjust the transmission rate. This figure indicates that our CS-SIQIM with DFISTA outperforms conventional OFDM and SIM at the moderate SNR region. However, CS-SIQIM has an error floor at high SNR region, as it can be predicted that this compression condition is severe with the parameters (N, M, K). On the other hand, it can be seen that the error floor is slightly lowered upon enlarging the compression size. Comparing AC-SIQIM(496,256,3) using DFISTA to the conventional SIM, about 15 dB gain is observed at BER=10^{-4}. With the aid of AC, the mutual coherence of the measurement matrix can be lowered upon enlarging the matrix size, so that the reconstruction performance of DFISTA was improved.

We further evaluate the BER performance of AC-SIQIM with high-order modulation, such as 16- and 64-ary quadrature amplitude modulation (QAM). To increase a modulation order, we employ 4- and 8-PAM on each in-phase and quadrature-phase in CS-SIQIM system.

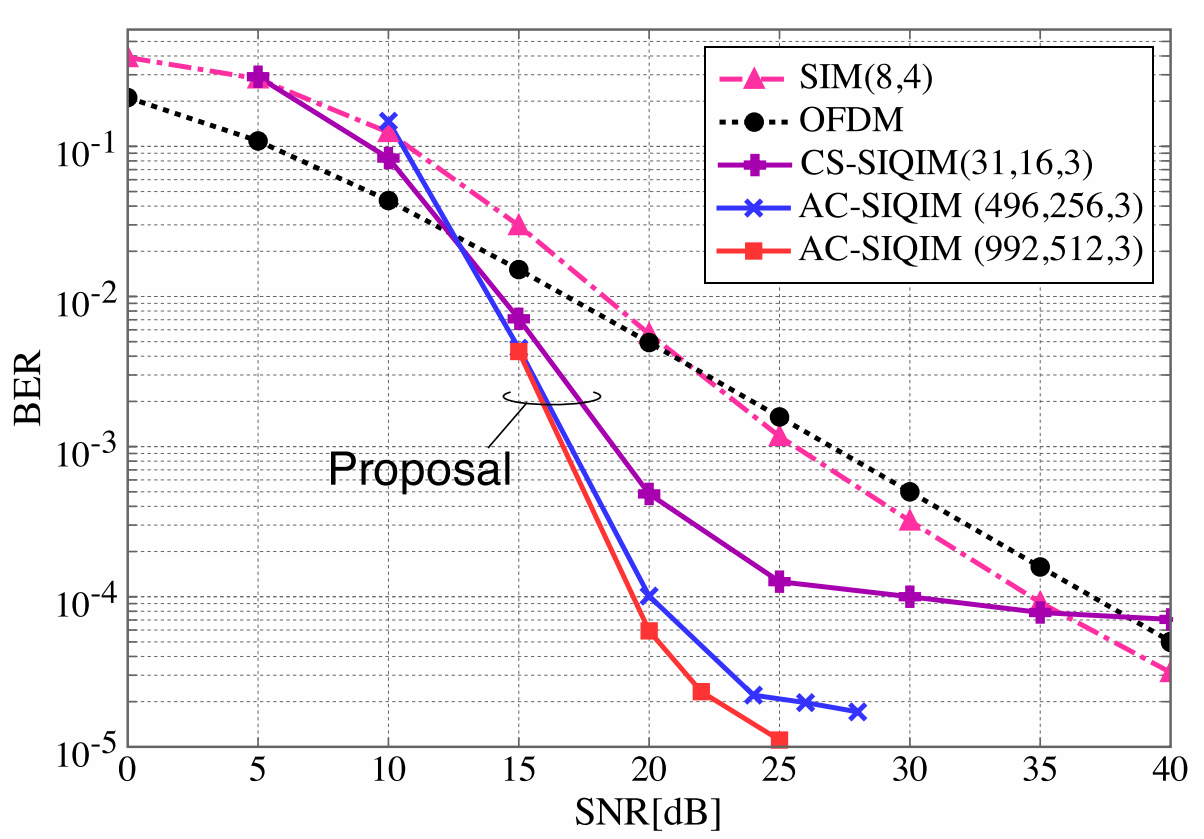

Figure 5.4: BER comparison of CS/AC-SIQIM with DFISTA and OFDM, where the transmission rates of CS/AC-SIQIM and OFDM are set as 1.875 bits/s/Hz, and that of SIM is set as 1.75 bits/s/Hz. The number of iteration in DFISTA is 100. JML detection is employed in SIM and OFDM.

Figure 5.5 shows the BER performances of OFDM and AC-SIQIM with 4-PAM and 8-PAM with DFISTA where (NG, M_{all}, K) is set as (496,256,2) in both schemes. This figure illustrates CS-SIQIM with 4-PAM is superior to OFDM with 16-QAM at high SNR region. Even though CS-SIQIM with 8-PAM exhibits the lower BER than OFDM, the waterfall region appears at higher SNR region than the case of 4-PAM due to the lower MED [4]

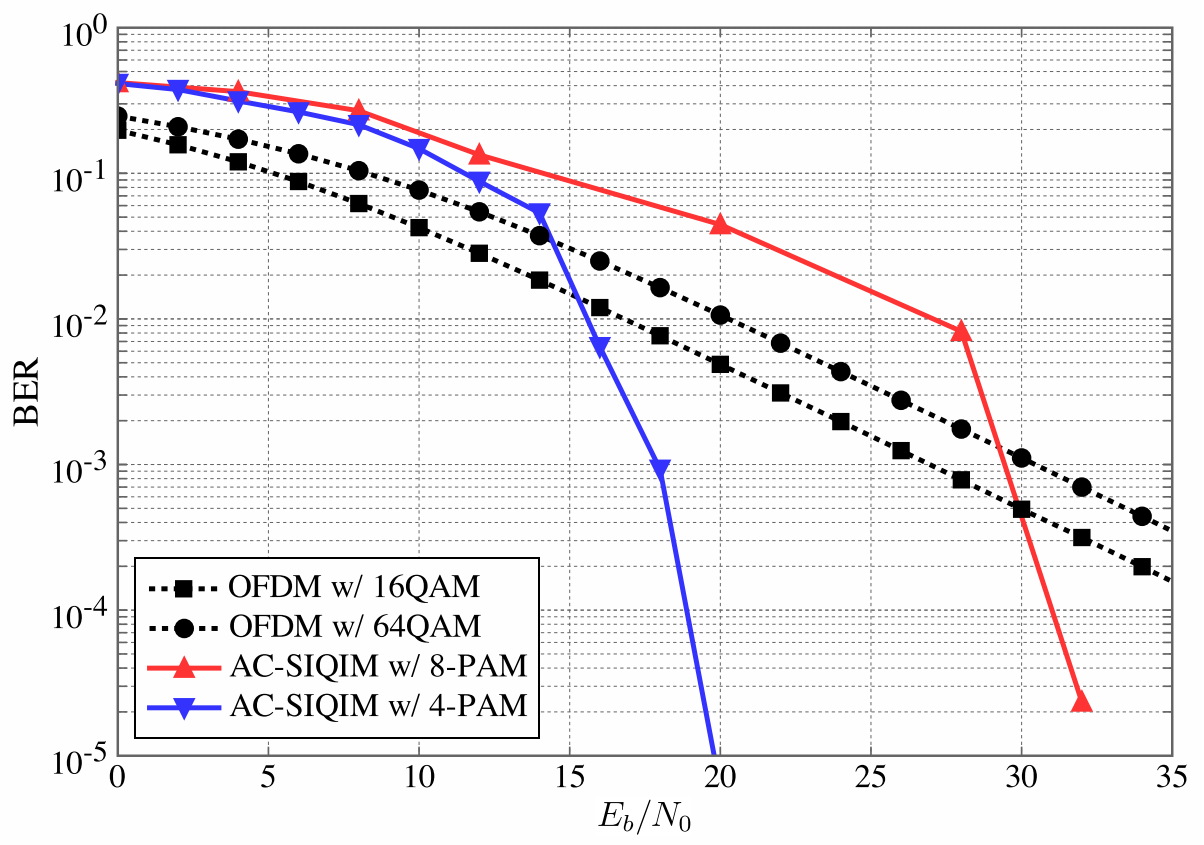

Figure 5.5: BER v.s. E_b/N_0 performances of CS-SIQIM relying on DFISTA with 4-PAM and 8PAM and OFDM with 16-QAM and 64-QAM, where (NG, M_{all}, K) is set as $(496, 256, 2)$. Transmission rates of OFDM with 16-QAM, 64-QAM and AC-SIQIM with 4-PAM, and 8-PAM are set as 4.0, 6.0, 1.5, and 1.75 bits/s/Hz, respectively.

Chapter 6

Conclusions

In this paper, we have proposed CS-SIQIM and AC-SIQIM relying on DFISTA and optimized hyperparameters in DFISTA via DE. It has been shown that our proposed detector has a constant complexity even as increasing the number of active subcarriers K, i.e., the transmission rate. In addition, our AC-SIQIM with DFISTA has been shown to be superior to CS-SIM with IRC detector in terms of its BER. Moreover, our solution has attained a higher performance than conventional OFDM and SIM. In our future work, we will consider channel coding and multi-user scenarios of CS-SIQIM.

Chapter 7

Bibliography

[1] R. Abu-alhiga and H. Haas, "Subcarrier-index modulation OFDM," in *2009 IEEE 20th International Symposium on Personal, Indoor and Mobile Radio Communications*, Sept. 2009, pp. 177–181.

[2] R. Mesleh, H. Haas, S. Sinanovic, C. W. Ahn, and S. Yun, "Spatial modulation," *IEEE Trans. Veh. Technol.*, vol. 57, no. 4, pp. 2228–2241, 2008.

[3] T. Datta, H. S. Eshwaraiah, and A. Chockalingam, "Generalized space-and-frequency index modulation," *IEEE Trans. Veh. Technol.*, vol. 65, no. 7, pp. 4911–4924, July 2016.

[4] N. Ishikawa, S. Sugiura, and L. Hanzo, "Subcarrier-index modulation aided OFDM - Will it work?" *IEEE Access*, vol. 4, pp. 2580–2593, 2016.

[5] Y. Xiao, S. Wang, L. Dan, X. Lei, P. Yang, and W. Xiang, "OFDM with interleaved subcarrier-index modulation," *IEEE Commun. Lett.*, vol. 18, no. 8, pp. 1447–1450, Aug. 2014.

[6] T. Mao, Z. Wang, Q. Wang, S. Chen, and L. Hanzo, "Dual-mode index modulation aided OFDM," *IEEE Access*, vol. 5, pp. 50–60, 2017.

[7] H. Zhang, L.-L. Yang, and L. Hanzo, "Compressed sensing improves the performance of subcarrier index-modulation assisted OFDM," *IEEE Access*, vol. 4, pp. 1–15, 2016.

[8] D. L. Donoho, "Compressed sensing," *IEEE Trans. Inf. Theory*, vol. 52, no. 4, pp. 1289–1306, Apr. 2006.

[9] R. Hayakawa and K. Hayashi, "Discreteness-aware AMP for reconstruction of symmetrically distributed discrete variables," in *2017 IEEE 18th International Workshop on Signal Process. Advances in Wireless Commun.*, 2017, pp. 1–5.

[10] ——, "Discreteness-aware approximate message passing for discrete-valued vector reconstruction," *IEEE Trans. Signal Process.*, vol. 66, no. 24, pp. 6443–6457, Dec. 2018.

[11] M. Nagahara, "Discrete signal reconstruction by sum of absolute values," *IEEE Signal Process. Lett.*, vol. 22, no. 10, pp. 1575–1579, Oct. 2015.

[12] D. L. Donoho, A. Maleki, and A. Montanari, "Message Passing Algorithms for Compressed Sensing," *2010 IEEE Inf. Theory Workshop on Inf. Theory*, pp. 1–5, 2009.

[13] A. Beck and M. Teboulle, "A fast iterative shrinkage-thresholding algorithm for linear inverse problems," *Society for Industrial and Applied Mathematics Journal on Imaging Sciences*, vol. 2, no. 1, pp. 183–202, 2009.

[14] H. Sasahara, K. Hayashi, and M. Nagahara, "Faster-than-Nyquist signaling by sum-of-absolute-values optimization," in *2016 SICE International Symposium on Control Systems (ISCS)*, Mar. 2016, pp. 7–8.

[15] L. R. Welch, "Lower bounds on the maximum cross correlation of signals," *IEEE Trans. Inf. Theory*, vol. 20, no. 3, pp. 397–399, May 1974.

[16] R. Storn and K. Price, "Differential evolution - a simple and efficient adaptive scheme for global optimization over continuous spaces," *ICSI, USA, Tech. Rep. TR-95-012*, 1995.

[17] E. Basar, U. Aygolu, E. Panayirci, and H. Poor, "Orthogonal frequency division multiplexing with index modulation," in *GLOBECOM - IEEE Global Telecommunications Conference*, vol. 61, no. 22, 2012, pp. 5536–5549.

[18] E. Basar, U. Aygolu, E. Panayirci, and H. V. Poor, "Orthogonal frequency division multiplexing with index modulation," *IEEE Trans. Signal Process.*, vol. 61, no. 22, pp. 5536–5549, Nov. 2013.

[19] K. Hayashi, M. Nagahara, and T. Tanaka, "A user's guide to compressed sensing for communications systems," *IEICE Trans. Commun.*, vol. E96-B, no. 3, pp. 685–712, Mar. 2013.

[20] A. M. Tillmann and M. E. Pfetsch, "The computational complexity of the restricted isometry property, the nullspace property, and related concepts in compressed sensing," *IEEE Trans. Inf. Theory*, vol. 60, no. 2, pp. 1248–1259, Feb. 2014.

[21] M. Wen, X. Cheng, S. Member, M. Ma, B. Jiao, and H. V. Poor, "On the achievable rate of OFDM with index modulation," *IEEE Trans. Signal Process.*, vol. 64, no. 8, pp. 1919–1932, 2016.

[22] A. Chockalingam and B. Sundar Rajan, *Large MIMO systems*. Cambridge University Press, 2014.

[23] H. Zhang, L.-L. Yang, and L. Hanzo, "Compressed impairment sensing assisted and interleaved-double-FFT aided modulation improves broadband power line communications subjected to asynchronous impulsive Noise," *IEEE Access*, vol. 3536, no. c, pp. 81–96, 2015.

[24] M. A. Figueiredo, J. M. Bioucas-Dias, and R. D. Nowak, "Majorization-minimization algorithms for wavelet-based image restoration," *IEEE Trans. Image Process.*, vol. 16, no. 12, pp. 2980–2991, 2007.

[25] H. Sasahara, K. Hayashi, and M. Nagahara, "Multiuser detection based on MAP estimation with sum-of-absolute-values relaxation," *IEEE Trans. Signal Process.*, vol. 65, no. 21, pp. 5621–5634, 2017.

[26] S. D. Li, F. W. Chen, J. Yang, and X. Y. Ma, "A NOVEL 2D COMPLEX FISTA FOR ISAR IMAGING," in *IET International Radar Conf. 2015*, Oct 2015, pp. 1–4.

Acknowledgments

This thesis consists of my master study at the University of Electro-Communications, Tokyo, Japan. I sincerely appreciate every support by people who contributed the master thesis, especially my supervisor, Associate Professor Koji Ishibashi, and Professor Takeo Fuji. Moreover, I would like to thank Associate Professor Shinsuke Ibi, who is with Department of Information and Communications Technology, Osaka University, for careful and insightful advice to my study. In addition, Professor Lajos Hanzo who is with The University of Southampton, U.K., supervised my study during the visiting to his laboratory, so that I deeply appreciate his advice and kindness. I'm also grateful to all the member of Advanced Wireless & Communication Research (AWCC) center. Finally, I would like to sincerely thank my family, Yuji, Kiyomi, and Hiroki.

List of Publications

International Conference (1)

1. K. Ohira, T. Hara, and K. Ishibashi, "Aggregate-compression-aided subcarrier IQ index modulation," in *Proceedings of 2018 15th Workshop on Positioning, Navigation and Communications (WPNC)*, Bremen, Germany, 25–26 October 2018, pp. 1–6.

Domestic Conference (3)

1. K. Ohira and K. Ishibashi, "Compressed-sensing-aided subcarrier IQ index modulation with discreteness-aware fast iterative shrinkage-thresholding algorithm ," in *IEICE Technical Report RCS2018-51*, vol. 118, no. 101, June 2018, pp. 95–100.

2. K. Ohira, T. Hara, and K. Ishibashi, "Aggregate-compression-aided subcarrier IQ index modulation with discreteness-aware approximate message passing ," in *IEICE Technical Report RCS2018-128*, vol. 118, no. 125, July 2018, pp. 243–248.

3. K. Ohira and K. Ishibashi, "Aggregate-compression-aided subcarrier IQ index modulation with discreteness-aware fast iterative shrinkage-thresholding algorithm," in *Proceedings of the Symposium on Information Theory and Its Applications*, December 2018, pp. 125–130.